The molecular products and biogeochemical significance of lipid photooxidation in West Antarctic surface waters

James R. Collins[a,b,*,1], Helen F. Fredricks[a], Jeff S. Bowman[c,2], Collin P. Ward[a], Carly Moreno[d], Krista Longnecker[a], Adrian Marchetti[d], Colleen M. Hansel[a], Hugh W. Ducklow[c], and Benjamin A. S. Van Mooy[a,*]

[a] Department of Marine Chemistry and Geochemistry, Woods Hole Oceanographic Institution, Woods Hole, MA 02543, USA

[b] MIT/WHOI Joint Program in Oceanography/Applied Ocean Science and Engineering, Woods Hole, MA 02543, USA

[c] Division of Biology and Paleo Environment, Lamont-Doherty Earth Observatory, Columbia University, Palisades, NY 10964, USA

[d] Department of Marine Sciences, University of North Carolina at Chapel Hill, Chapel Hill, NC 27599, USA

* Corresponding authors. *E-mail addresses:* james.r.collins@aya.yale.edu (James R. Collins), bvanmooy@whoi.edu (Benjamin A. S. Van Mooy).

[1] Present address: School of Oceanography and eScience Institute, University of Washington, Seattle, WA 98195, USA.

[2] Present address: Scripps Institution of Oceanography, University of California, San Diego, La Jolla, CA 92093, USA

Abstract

The seasonal depletion of stratospheric ozone over the Southern Hemisphere allows abnormally high doses of ultraviolet radiation (UVR) to reach surface waters of the West Antarctic Peninsula (WAP) in the austral spring, creating a natural laboratory for the study of lipid photooxidation in the shallow mixed layer of the marginal ice zone. The photooxidation of lipids under such conditions has been identified as a significant source of stress to microorganisms, and short-chain fatty acids altered by photochemical processes have been found in both marine aerosols and sinking marine particle material. However, the biogeochemical impact of lipid photooxidation has not been quantitatively compared at ecosystem scale to the many other biological and abiotic processes that can transform particulate organic matter in the surface ocean. We combined results from field experiments with diverse environmental data, including high-resolution, accurate-mass HPLC-ESI-MS analysis of lipid extracts and *in situ* measurements of ultraviolet irradiance, to address several unresolved questions about lipid photooxidation in the marine environment. In our experiments, we used liposomes — nonliving, cell-like aggregations of lipids — to examine the photolability of various moieties of the intact polar diacylglycerol (IP-DAG) phosphatidylcholine (PC), a structural component of membranes in a broad range of microorganisms. We observed significant rates of photooxidation only when the molecule contained the polyunsaturated fatty acid (PUFA) docosahexaenoic acid (DHA). As the DHA-containing lipid was oxidized, we observed the steady ingrowth of a diversity of oxylipins and oxidized IP-DAG; our results suggest both the intact IP-DAG the degradation products were amenable to heterotrophic assimilation. To complement our experiments, we used an enhanced version of a new lipidomics discovery software package to identify the lipids in water column samples and in several diatom isolates. The galactolipid digalactosyldiacylglycerol (DGDG), the sulfolipid sulfoquinovosyldiacylglycerol (SQDG) and the phospholipids PC and phosphatidylglycerol (PG) accounted for the majority of IP-DAG in the water column particulate (≥ 0.2 µm) size fraction; between 3.4 and 5.3 % of the IP-DAG contained fatty acids that were both highly polyunsaturated (i.e., each containing ≥ 5 double bonds). Using a broadband apparent quantum yield

2

(AQY) that accounted for direct and Type I (i.e., radical-mediated) photooxidation of PUFA-containing IP-DAG, we estimated that 0.7 ± 0.2 μmol IP-DAG m^{-2} d^{-1} (0.5 ± 0.1 mg C m^{-2} d^{-1}) were oxidized by photochemical processes in the mixed layer. This rate represented 4.4 % (range, 3-21 %) of the mean bacterial production rate measured in the same waters immediately following the retreat of the sea ice. Because our liposome experiments were not designed to account for oxidation by Type II photosensitized processes that often dominate in marine phytodetritus, our rate estimates may represent a sizeable underestimate of the true rate of lipid photooxidation in the water column. While production of such diverse oxidized lipids and oxylipins has been previously observed in terrestrial plants and mammals in response to biological stressors such as disease, we show here that a similar suite of molecules can be produced via an abiotic process in the environment and that the effect can be commensurate in magnitude with other ecosystem-scale biogeochemical processes.

Abbreviations

AQY	Apparent quantum yield
BHT	Butylated hydroxytoluene
DCM	Dichloromethane
DGCC	Diacylglyceryl carboxyhydroxymethylcholine
DGDG	Digalactosyldiacylglycerol
DGTA	Diacylglyceryl hydroxymethyl-trimethyl-β-alanine
DGTS	Diacylglyceryl trimethylhomoserine
DHA	Docosahexaenoic acid
DNP-PE	Dinitrophenyl-phosphatidylethanolamine
ESI	Electrospray ionization
FFA	Free fatty acid
FSFA	Fully saturated fatty acid
GlyPCho	Glycerophosphocholine
HAc	Acetic acid
HPLC	High-performance liquid chromatography
IP-DAG	Intact polar diacylglycerol
IPL	Intact polar lipid
LPC	Lysophosphatidycholine
MeOH	Methanol
MDA	Malondialdehyde
MGDG	Monogalactosyldiacylglycerol
MUFA	Monounsaturated fatty acid
DUFA	Diunsaturated fatty acid
Ox-IPL	Oxidized intact polar lipid
Ox-PC	Oxidized phosphatidylcholine
PC	Phosphatidylcholine
PCho	Phosphocholine
PE	Phosphatidylethanolamine
PG	Phosphatidylglycerol
PTFE	Polytetrafluoroethylene
PUFA	Polyunsaturated fatty acid
SQDG	Sulfoquinovosyldiacylglycerol
TAG	Triacylglycerol
TBA	Thiobarbituric acid
Tris	Tris(hydroxymethyl)aminomethane
UVA	Ultraviolet-A (315-400 nm)
UVB	Ultraviolet-B (290-315 nm)
UVR	Ultraviolet radiation

1.   Introduction

The seasonal depletion of stratospheric ozone over the Southern Hemisphere continues to allow abnormally high doses of ultraviolet radiation (UVR) to reach the land and ocean surface in much of Antarctica (IPCC, 2005; Laube et al., 2014). The negative effects of UVR on marine plankton are mediated primarily via reactive oxygen species (ROS) and include shifts in bulk cellular lipid composition, reduced cell growth rates, direct damage to critical biochemicals such as DNA and proteins (Moreau et al., 2016; Worrest, 1983), and cell mortality (Davidson et al., 1994; Davidson and Marchant, 1994; Helbling et al., 1996; Hessen et al., 1997; Karentz, 1994; Mock and Kroon, 2002; Neale et al., 1994; Prézelin et al., 1994; Skerratt et al., 1998; Vernet et al., 1994). In the West Antarctic Peninsula (WAP) specifically, UVR exposure has been correlated with declines in marine primary production (Schofield et al., 1995).

ROS can also oxidize and damage acyl-containing lipids such as intact polar diacylglycerols (IP-DAG), the primary structural components of many cell and organelle membranes (Crastes de Paulet et al., 1988; Kramer et al., 1991; Murphy, 1983). Diatoms and other phytoplankton that inhabit high-latitude waters such as those of the WAP may contain as much as 30 % lipid; this lipidome is often dominated by IP-DAG containing polyunsaturated fatty acids (PUFA, i.e., those containing ≥ 2 double bonds; Nichols et al., 1989; Palmisano et al., 1988; Skerratt et al., 1998), which are particularly susceptible to peroxidation (Girotti, 1990, 1998; Wagner et al., 1994). Laboratory studies and experiments in other environmental systems have shown that peroxidation of PUFA can produce hundreds of bioactive lipid derivatives, collectively termed oxylipins. Oxylipins of enzymatic origin are known to play critical roles as intercellular signals, stress mediators, and predator defense mechanisms in various diatoms isolated from mid-latitude ecosystems (Barofsky and Pohnert, 2007; Fontana et al., 2007; Lauritano et al., 2011; Lauritano et al., 2012; Leflaive and Ten-Hage, 2009; Miralto et al., 1999; Wichard et al., 2005); these molecules can also affect growth rates of marine heterotrophic bacteria (Ribalet et al., 2008) and regulate metabolism of bacteria associated with sinking particles (Edwards et al.,

2015). Various diatoms typically dominate sea-ice and ice-edge communities during early stages of blooms in Antarctic waters (Lizotte, 2001).

While the biological production and bioactivity of diatom-derived oxylipins has received significant scientific attention in oceanography and UVR-induced oxylipin production has been characterized in higher plants and other organisms (Girotti, 1990, 1998; Halliwell and Chirico, 1993), the non-enzymatic generation of oxylipins and other oxidized lipid derivatives in the environment has received comparatively little scientific attention. Neither the biological nor abiotic production of larger oxidized lipid products such as intact oxidized polar lipids (ox-IPL; e.g., Buseman et al., 2006; Domingues et al., 2008; O'Donnell, 2011; Spickett and Pitt, 2015; Vu et al., 2012) has been investigated in the ocean or other natural environment. Rontani and others (Christodoulou et al., 2010; Marchand and Rontani, 2001; Rontani, 1999, 2001; Rontani et al., 2016; Rontani et al., 2012a; Rontani et al., 2012b; Rontani et al., 1998) have established that Type II (i.e., involving singlet oxygen) photooxidation of mono- and di-unsaturated fatty acids in phytodetritus is a process significant enough to be detected via short-chain oxylipin biomarkers in sinking marine particulate material, but the photooxidation of intact polar lipids in high-latitude marine microbial biomass has not been directly investigated. In addition, while short-chain fatty acids altered by photochemical processes have been used to estimate the photooxidation state of organic matter in sinking marine particles in the Arctic (Amiraux et al., 2017; Rontani, 1999; Rontani et al., 2012a) and carboxylic acids of photochemical origin have been previously identified in marine aerosols (Kawamura and Gagosian, 1987; Kawamura and Gagosian, 1990), few estimates exist of the relative biogeochemical impact of lipid photooxidation in the surface ocean compared to the many other biological and abiotic processes that can transform particulate organic matter.

In this study, we combined results from experiments in a model liposome system with diverse environmental data, including high-resolution, accurate-mass high performance liquid chromatography-electrospray ionization mass spectrometry (HPLC-ESI-MS) analysis of lipid samples and *in situ* time-

series measurements of ultraviolet irradiance, to address several research objectives that spanned molecular to ecosystem scales. First, we sought to determine whether the photooxidation of IP-DAG was dependent on molecular structure — i.e., would a higher degree of unsaturation in the fatty acids of a particular molecule make it more amenable to photooxidation under natural environmental conditions? Second, we sought to test two closely entwined hypotheses regarding the relationship between lipid biogeochemistry and heterotrophic bacterial metabolism, namely that (1) bacterial metabolism of intact lipids present in the added liposomes would enhance apparent overall degradation rates as the organisms responded to the addition of a new potential carbon source; and, conversely, that (2) photodegradation of the lipids into smaller, less complex metabolites would provide new, bioavailable substrates for the bacteria (as proposed, e.g., in Karl and Resing, 1993; D. J. Kieber et al., 1989). Third, we sought to characterize the diversity, quantities, and structures of various products of lipid photooxidation by applying an enhanced version of the lipidomics data analysis package described in Collins et al. (2016) to HPLC-ESI-MS data from our liposome experiments. We then applied the lipidomics workflow to characterize the lipidomes of plankton from the WAP water column and determine what fraction of the particulate (≥ 0.2 μm) lipid biomass would likely be amenable to degradation by photooxidation. Finally, we combined our various measurements to calculate a broadband apparent quantum yield (AQY) for photooxidation of IP-DAG by direct and Type I (i.e., radical-mediated) mechanisms. To complete our analysis, we applied this AQY to the water column lipid data to estimate the minimum rate of lipid photooxidation within the carbon cycle of the WAP ecosystem.

2.   Methods

2.1.   Ultraviolet photooxidation experiments

Five lipid photooxidation experiments were conducted in the austral spring of 2013 under natural sunlight at Palmer Station, a U.S. Antarctic Program facility on Anvers Island, West Antarctica (64°46'27" S, 64°03'11" W; Fig. 1). In the experiments, liposomes of various species of phosphatidylcholine (PC) — a membrane lipid common to nearly all phyla, including marine microbial

eukaryotes and prokaryotes — were exposed to natural doses of incoming ultraviolet radiation in a large, outdoor aquarium at 0.6 m water depth (Table A1; Fig. A2). Mixtures of liposomes were incubated in quartz glass vials representing various light and microbial community treatments while incoming solar radiation was measured *in situ* at the center of aquarium; samples were sacrificed in triplicate at predesignated time points and the lipid content recovered by liquid-liquid extraction. The two microbial community treatments were achieved by filtering the seawater matrix in which the liposomes were suspended to either 0.2 or 0.7 μm (treatments referred to hereafter as "- het. bact." and "+ het. bact.," respectively). Dark controls were covered in foil and maintained in a darkened incubator at the same temperature as the aquarium. The experimental design is further described in the Appendix.

We employed additional assays during two experiments to (1) validate our observations of lipid photooxidation with a standard measurement of lipid peroxidation and (2) interrogate bacterial metabolic activity in our + het. bact. treatments (i.e., those containing the 0.7 μm seawater filtrate). First, we adapted a commercial biomedical assay kit (Lipid Peroxidation/MDA Assay Kit ab118970; Abcam Inc., Cambridge, UK) to detect the presence in our samples of malondialdehyde (MDA), a low-molecular-weight oxidation end-product of both enzymatically catalyzed (Armstrong and Browne, 1994) and abiotic (Janero, 1990) lipid peroxidation in a variety of organisms. In addition, activities of four bacterial exoenzymes (lipase, alkaline phosphatase, α-D-glucosidase, and L-Leucine-4-methylcoumaryl-7-amide, or leu-MCA) were monitored throughout the experiments using a series of fluorogenic substrates (Hoppe, 1993) as described in Edwards et al. (2011; details, Appendix, Section A.1.5). Rates of bacterial production (i.e., the synthesis of biomass by heterotrophic bacterioplankton) were determined as part of the PAL-LTER study using the microcentrifuge ^{3}H-leucine incorporation method described in Ducklow et al. (2012), which is a modification of the assay introduced by Smith and Azam (1992).

2.2.   Measurements of incoming irradiance

A continuous time series of incident irradiances ($I_{0+}(\lambda)$) was collected with a SUV-100

spectroradiometer (Biospherical Instruments Inc., San Diego, CA, USA) as part of the U.S. National Oceanic and Atmospheric Administration's (NOAA) Antarctic UV Monitoring Network (Bernhard et al., 2005; 2010; Fig. 2). Separately, during the photooxidation experiments, an Ocean Optics Jaz spectrometer suspended in the outdoor aquarium was used to record downwelling irradiances *in situ* (ILX-511B detector; 0.3 nm bandwidth from 200-850 nm; Ocean Optics Inc., Dunedin, FL, USA). The Jaz was also used to make several downwelling irradiance profiles in the water column adjacent to Palmer Station in Arthur Harbor; these profile data were used to calculate a series of downwelling attenuation coefficients, $K_d(\lambda)$ (Fig. A3). The $K_d(\lambda)$ were then combined with incident SUV-100 data to estimate daily UVB and UVA radiation doses received at 0.6 m (Fig. 2, dashed trace) and at multiple depths through the mixed layer (details, Appendix, Section A.2). We confirmed the accuracy of these dose estimates using doses calculated independently from *in situ* data from the Jaz device (Fig. 2, open circles).

2.3. Benchtop absorbance and transmissivity measurements

Wavelength-specific absorbances of various PC lipid standards and surface seawater samples from Arthur Harbor were measured in the laboratory using a dual-path UV-visible spectrophotometer (Thermo Nicolet Evolution 300; ThermoFisher Scientific; details, Appendix, Section A.3). Absorbance spectra of the standards were used to calculate a series of wavelength-specific molar decadic absorption coefficients ($\varepsilon_i(\lambda)$, in units of M^{-1} cm^{-1}; Fig. A4). The seawater absorbances were used to calculate wavelength-specific absorption coefficients ($\alpha_{SW}(\lambda)$, in units of m^{-1}; Fig. A5).

2.4. Water column sample collection

In addition to the photooxidation experiments, water samples were collected for lipid analysis from Arthur Harbor (at LTER Station B; Fig. 1b) and at stations offshore (PAL-LTER cruise LMG1401 aboard the ARSV *Laurence M. Gould*). Samples for analysis of particulate (i.e., cell-bound) lipids were retrieved from depth using standard oceanographic sampling equipment and then collected by vacuum filtration onto 0.2 μm pore size Durapore membrane filters; these were frozen immediately at −

80°C. Extraction was performed using a modified Bligh and Dyer (Bligh and Dyer, 1959) method described in Popendorf et al. (2013). Extracts were processed and then stored at –80°C.

2.5. High-resolution HPLC-ESI-MS analysis

Lipid extracts were analyzed by HPLC-ESI-MS using a high-resolution, accurate-mass Thermo Q Exactive Hybrid Quadrupole-Orbitrap mass spectrometer with data dependent-MS^2 acquisition (ThermoFisher Scientific, Waltham, MA, USA) coupled to an Agilent 1200 HPLC system (Agilent, Santa Clara, CA, USA). Chromatographic conditions were modified from Hummel et al. (2011). The full MS method is described in Section A.5 of the Appendix; we achieved an effective mass accuracy of < 0.2 ppm, as reported in Collins et al. (2016).

2.5.1. *Identification and quantification of lipids & oxidized lipids*

All HPLC-ESI-MS data were analyzed in R (R Core Team, 2016) using open-source tools according to the lipidomics workflow described in Collins et al. (2016). The LOBSTAHS lipidomics discovery software (Collins et al., 2016) was used to putatively identify the processed, high-quality MS features based on exact mass, retention time, and diagnostic adduct hierarchy. Full details of the MS data analysis, including the criteria we used to confirm the identities of the lipids in each dataset and our quantification methods, are described in Section A.5.4 of the Appendix; LOBSTAHS identifies TAG and IP-DAG by the "sum composition" (Husen et al., 2013) of double bonds and acyl carbon atoms in each compound (e.g., PC 34:1, rather than PC 16:0–18:1). Our approach allowed us to identify and quantify the intact PC species in our experiments with a high level of confidence falling somewhere between levels 1 and 2 in the proposed scheme of Sumner et al. (2007) for metabolite identification. For compounds identified in the water column data, we confirmed all LOBSTAHS identities using a new software feature that automatically detects diagnostic product ion fragments and constant neutral losses for each lipid class (as given in Popendorf et al., 2013) in the available data-dependent MS^2 spectra for each sample, allowing us to achieve a confidence approaching level 2 in the Sumner et al. (2007) scheme.

2.6. Broadband apparent quantum yield (AQY) calculation

We combined the removal rates (where observed) of PC species determined in the liposome experiments, *in situ* photon irradiance measurements, and other parameters described above and in the Appendix to calculate a broadband apparent quantum yield, Φ_{UVR}, for photooxidation of lipids by radiation received between 290-395.5 nm, where

$$\Phi_{UVR} = \frac{\text{moles of a given lipid } i \text{ transformed}}{\begin{array}{c}\text{moles of photons between 290 and 395.5 nm}\\ \text{absorbed by lipids in system}\end{array}} \qquad (1)$$

The adoption of a broadband AQY is consistent with previous work in which maximum degradation rates of polyunsaturated lipids in senescent phytoplanktonic cells were induced by exposure to a broad spectrum that spanned the UV and visible wavebands (Christodoulou et al., 2010; Rontani et al., 1998). We calculated the broadband AQY of a given lipid i according to the equation (modified from Miller (1998) and Cory et al. (2014)):

$$\frac{-d[i]}{dt} = \Phi_{UVR} \int_{290}^{395.5} \frac{E_{n,p,\Sigma}(\lambda)T(\lambda)\left(1-e^{-\alpha_{tot}(\lambda)z_{eff}}\right)}{z_{eff}} F_i(\lambda)d\lambda \qquad (2)$$

where $-d[i]/dt$ is the appropriate change in concentration of lipid i; Φ_{UVR} is the broadband AQY in units of mol (mol photons)$^{-1}$; $E_{n,p,\Sigma}(\lambda)$ is the total number of photons of wavelength λ received per unit area over the course of the experiment (from the *in situ* spectrophotometer data), $T(\lambda)$ is the transmissivity (as a fraction) of the incubation vessel wall material at wavelength λ; $\alpha_{tot}(\lambda)$ is the absorptivity at wavelength λ of all components in the experimental system (filtered seawater, lipid i and other lipids present), expressed as a linear Napierian absorption coefficient (m^{-1}); z_{eff} is the effective optical pathlength within the quartz vials during the experiment; and $F_i(\lambda)$ is the fraction of light absorbed within the system at wavelength λ by lipid i. Calculation of $\alpha_{tot}(\lambda)$ and $F_i(\lambda)$ are described in Section A.6.1 of the Appendix. We defined z_{eff} as the inner diameter of the incubation vials (1.8 cm) since the vessels were left to rest on their sides during the experiments and were exposed to sunlight from above. We defined $-d[i]/dt$ as the change in concentration of PC 22:6, 22:6 observed in the + UVR treatment relative to the change in the dark control, assuming that the change in concentration in the

latter represented the baseline rate of autooxidation. A series of Monte Carlo simulations was used to determine the uncertainty in the AQY (Collins et al., 2015; details, Appendix, Section, A.6.2).

2.6.1. *Potential sources of bias in method used to calculate AQY*

We considered several potential sources of bias in the method we used to calculate the AQY. First, there is some evidence to challenge our assumption that the rate of oxidation observed in dark controls can be used represent the baseline rate of autooxidation. For example, irradiation in some cases can produce peroxides, homolytic cleavage of which can induce autooxidation in cells (Girotti, 1998). Our estimates of $-d[i]/dt$ may therefore include contributions from light-induced autooxidative processes. Second, because it can be difficult to determine the optical pathlength in a curved vessel (Vähätalo et al., 2000), we conducted a follow-up experiment to compare irradiances from the *in situ* spectrophotometer data (Eq. 2, term under integral sign) to those measured directly in quartz glass vials using chemical actinometry (Jankowski et al., 1999; D. J. Kieber et al., 2007). Consistent with previous findings (D. J. Kieber et al., 2007), the actinometer-derived irradiance for the 330-380 nm spectral band was not significantly different from the integrated irradiance we calculated from the Jaz data (Appendix, Section A.2.4). Third, since our liposome suspensions did not contain Type II photosensitizers such as chlorophyll, we presumed very little singlet oxygen was produced photochemically during our experiments (further discussion, Section 4.4). We thus concluded that our AQY likely accounted only for photooxidation by Type I (i.e., radical-mediated) processes, any light-induced autooxidative processes that were not accounted for through the use of dark controls and, to a lesser extent, some direct initiation by UVR.

2.7. Lipid photooxidation rate estimates for natural waters of West Antarctica

Finally, we estimated rates of lipid photooxidation in natural waters of the West Antarctic Peninsula ($-d[lipid]/dt$; units of pmol lipid $L^{-1} d^{-1}$ or pmol C $L^{-1} d^{-1}$) by combining the broadband AQY calculated in Eq. 2 with estimates of subsurface irradiance and measured concentrations of specific lipids. Rates were estimated for two fractions of particulate lipids in WAP waters: IP-DAG containing (1) polyunsaturated (i.e., ≥ 3 double bonds) and (2) highly polyunsaturated (i.e., ≥ 5 double bonds) fatty

acids at both positions (*sn*-1 and *sn*-2) on the IP-DAG glycerol backbone. Volumetric rate estimates for each 1 m interval in the mixed layer were integrated to yield areal estimates of the photooxidation rate for each day during the study period. Details of calculations, including necessary equations, are presented in Section A.7 of the Appendix. Absent published data on the wavelength-dependence of photooxidation reactions in IP-DAG, we assumed (as in, e.g., Fichot and Benner, 2014) that the broadband Φ_{UVR} we calculated in Eq. 2 could be applied across the entire 290-395.5 nm waveband.

3.   Results

3.1.   Irradiance observations; UV penetration through shallow mixed layer

Temperature and salinity profiles showed that the mixed layer depth (MLD) remained between 5 and 10 m through the end of December 2013 (Fig. A6, Table A2). These conditions were indicative of a highly coherent, early summer surface "lens" (Perrette et al., 2011; Smith and Nelson, 1985, 1986) that served to expose the entire mixed layer to high doses of UVR. For example, 4.3 % of the incident radiation received at 320 nm was still present at a depth of 8 m (Fig. A3). Comparison of incident SUV-100 irradiance data (Fig. 2a, solid trace) with estimated downwelling doses of UVB radiation at 0.6 m water depth (Fig. 2a, dashed trace) indicated that 71 ± 0.7 % of UVB radiation received at the earth's surface reached the 0.6 m depth at which we conducted our experiments (mean ± SD; n = 76 daily calculations). We validated the accuracy of our $K_d(\lambda)$-derived UVB dose estimates by comparing them to daily doses calculated directly from *in situ* measurements with the Jaz spectrometer. We observed close agreement between the two methods; comparison of the *in situ* doses (Fig. 2a, open circles) to the incident SUV-100 data (Fig. 2a, solid trace) indicated that 73 ± 9 % of incoming UVB radiation was still present at 0.6 m (mean ± SD; n = 30 daily *in situ* dose estimates).

3.2.   Photooxidation of phosphatidylcholine liposomes

We obtained statistically significant results in our UVR-exposure experiments for only one of the seven PC moieties we considered: PC 22:6, 22:6 (*all-cis*-Δ^4,Δ^7,Δ^{10},Δ^{13},Δ^{16},Δ^{19}) (Fig. 3a, showing results from experiment on 14 December 2013; Table 1; Table A1). Changes in concentration of −804 ± 188 and

−827 ± 190 pmol mL^{-1} (mean ± SE) were observed in the + UVR - het. bact., and + UVR + het. bact. treatments, respectively, compared with a change of −322 ± 229 pmol mL^{-1} in the −het bact. dark control ($p ≤ 0.05$, Tukey's Honest Significant Difference method with α = 0.05; Table 1, Fig. 3a). Results from parallel + UVR - het. bact. incubations conducted in borosilicate glass vials were statistically indistinguishable from those in the quartz vials (Table A1). The consistently negative results we observed in the six other molecular species were confirmed in each case in at least two independent experiments (Table A1). Using the results from the 14 December experiment and the methods described in Section 2.6, we estimated a broadband AQY Φ_{UVR} for direct and Type I (i.e., radical-mediated) photooxidation of PUFA-containing IP-DAG of $0.54^{+0.26}_{-0.27}$.

3.3.   Photodegradation products putatively identified by HPLC-ESI-MS

High-resolution HPLC-ESI-MS data indicated that removal of unoxidized PC 22:6, 22:6 via photooxidation was accompanied by statistically significant rates of ingrowth of several unoxidized and oxidized derivatives (Fig. 4, Fig. 5a; Table 1). The former category included picomolar concentrations of lysophosphatidylcholine (LPC), while the latter included ox-PC species, oxylipins, and several ox-LPC species. The application of an unsupervised clustering algorithm to the data showed that changes in concentration of the various compounds were indicative of expected similarities between both treatments and timepoints (Fig. 4). Analysis of extracted ion chromatograms and data-dependent MS^2 spectra allowed us to putatively identify a series of progressively more oxidized ox-PC species in a representative + UVR - het. bact. sample at the final experimental timepoint (Fig. 5, Fig. 6, Fig. A7). We also observed a decrease in RT of each analyte in the series in proportion to the number of additional oxygen atoms it contained (Fig. 5b-d; Table 1). Further increasing our confidence, an analogous relationship between RT and oxidation state was noted for each of the other types of oxidized species we putatively identified (i.e., ox-LPC and the oxidized free fatty acid derivatives; Table 1). Our HPLC-ESI-MS observations of oxidized lipid production were also supported by measurements of MDA production obtained using a

commercial assay kit. Higher concentrations of MDA were observed in both + UVR treatments at t +8 h compared to the dark control ($p \leq 0.01$, Tukey HSD method; Fig. 3c); these concentrations were of the same order of magnitude as the concentrations of most of the more specific oxidation products we identified in the same samples using our high-resolution HPLC-ESI-MS method (Fig. 3b, Fig. 4).

Unique ions observed in the MS^2 spectra for each putatively identified feature (Fig. 6, Fig. A7) indicated either that (a) various positional isomers of each oxidized lipid were present, or (b) the exact nature of the oxidation was different in each case (e.g., the addition of two hydroxyl groups would yield ions of the same m/z as one featuring a single hydroperoxy functional group). These unique fragments were distinguished from the common headgroup fragments characteristic of the PC lipid class and other fragments, such as those representing unoxidized DHA, which were present in nearly all of the species (Fig. 6, Fig. A7). Based on previous findings (Milic et al., 2012; O'Donnell, 2011; Reis and Spickett, 2012; Sala et al., 2015; Spickett et al., 2011), it is likely the apparent diversity of species within each oxidized lipid class reflects a combination of the two situations. We suspect that the compound, non-Gaussian peak shapes we observed for the PC 22:6, 22:6 +2O and PC 22:6, 22:6 +4O species (Fig. 5c,d) indicate the presence of multiple, near-co-eluting ox-PC regioisomers (i.e., species with same oxidation state and type of oxidized functional group; Domingues et al., 2009; Reis et al., 2005). The presence of multiple isomers of each oxidized species in the sample is highly probable, given the multiple *bis*-allylic positions in the parent molecule and the nonselective, abiotic origin of the peroxidation. Far fewer positional isomers are produced in the case of biologically-mediated PUFA peroxidation; this is because the lipoxygenase enzymes responsible for production of short-chain oxylipins tend to have high affinity for specific positions in the acyl chains of their target substrate (Andreou and Feussner, 2009; Brash, 1999; Cutignano et al., 2011; Feussner and Wasternack, 2002).

3.4.   Distributions and acyl saturation state of IP-DAG in samples from waters of the West Antarctic Peninsula

We next sought to identify the lipids present in five samples of particulate organic matter (≥ 0.2 µm) collected from WAP surface waters during the austral spring of 2013-2014. Of the 4,393 different unoxidized and oxidized lipids we putatively identified in the five samples, we used response factors determined from authentic standards to quantify 318 definitively identified molecules in a subset that encompassed seven different classes of IP-DAG; statistics describing the performance of our multiple-step identification method are given in Table A5. Triacylglycerols (TAG) accounted for the vast majority (70.0 ± 8.8 %, mean ± SD) of the total identifiable lipid peak area in the five samples; in one sample (chromatogram, Fig. A8), TAG accounted for 83 % of the total peak area (Table A5). Results from three samples representative of different bloom conditions (Fig. 7, Fig. 8) indicated that species of the galactolipid DGDG, one of the four primary IP-DAG in the chloroplast membranes of photosynthetic organisms, accounted for the majority of the intact polar lipids we quantified in the data using authentic standards. Micromolar quantities of the sulfolipid SQDG and the phospholipids PC and PG were also present (Fig. 7). We also identified several species of diacylglyceryl carboxyhydroxymethylcholine (DGCC) in the samples; these were excluded from the dataset used to generate the figure because we did not have a suitable authentic standard available at the time of analysis. DGCC accounted for < 11 % of the total raw IP-DAG peak area in the Station E and CTD 27 samples, and 26.1 % of the total IP-DAG peak area in the sample from CTD 6. We also putatively identified several oxidized lipid species in the water column samples; these included all of the intact oxidized degradation products of PC 22:6, 22:6 that had we observed in our liposome experiments. Features representing PC 22:6, 22:6 +1O (two obvious isomers), PC 22:6, 22:6 +2O, PC 22:6, 22:6 +3O, and PC 22:6, 22:6 +4O were detected at 7.2, 3.9, 5.1, 0.5, and 0.8 %, respectively, of the abundance of PC 22:6, 22:6 (percentages are average values across the five samples; a link to the full, annotated list of all identified compounds and their raw chromatographic peak areas is included in the Appendix).

As a second means of analysis, we binned the IP-DAG species in each water column sample into five categories based on the saturation state of their attached fatty acids (Fig. 8). Molecular species

containing highly polyunsaturated fatty acids (i.e., those with ≥ 5 double bonds) at both substituent positions accounted for 5.3, 2.3, and 3.4 % of the IP-DAG in samples from PAL-LTER Station E and LMG 14-01 CTD stations 6 and 27, respectively (percentages calculated on basis of molar concentration; Fig. 8a; stations 6 and 27 correspond to LTER Grid locations 610.040 and 200.-060). Lipids containing two fatty acids of moderate polyunsaturation (i.e., ≥ 3 but < 5 double bonds) accounted for 31.1, 12.7, and 18.2 % of IP-DAG in the three samples. When we examined the acyl saturation state of molecular species belonging to single classes of IP-DAG, it became apparent that PUFA were not evenly distributed throughout the WAP metalipidome (e.g., PUFA were concentrated more heavily in species of PC than in the IP-DAG pool as a whole; Fig. 8b). Comparison of these results with a similar analysis of fatty acid distribution among IP-DAG classes in the four diatom isolates (Fig. A10) showed that the lipids of these diatoms did not dictate the composition of the overall WAP lipid pool, despite diatoms being traditionally responsible for many of the early-season blooms that occur in Antarctic waters (Nichols et al., 1989; Smith, 1987; Smith and Nelson, 1986).

4. Discussion

4.1. Dependence of photolability on acyl polyunsaturation

To our knowledge, rates of photooxidation have not been previously reported for IP-DAGs in natural waters. However, our observation that highly polyunsaturated fatty acids such as DHA are the primary target of photooxidation within these important molecules (Fig. 3; Table 1; Table A1) is consistent with well-established chemical models and several previous laboratory studies that evaluated the reactivity of free fatty acids in the presence of various reactive oxygen species (Cosgrove et al., 1987; Gardner, 1989; Schaich, 2005; Wagner et al., 1994). For example, Wagner et al. (1994) found that the addition of each new double bond which created a *bis*-allylic carbon atom increased exponentially the rate at which a given fatty acid was oxidized. However, these previous studies have focused almost exclusively on the reactivities of free fatty acids, largely ignoring intact lipids such as the IP-DAG we investigated in this study; our results demonstrate for the first time a direct relationship between acyl unsaturation and

photoreactivity in IP-DAG. Our findings do mirror those from two previous studies (R. J. Kieber et al., 1997; Rontani et al., 1998) in which the photoreactivities of various PUFA were evaluated under environmentally relevant light intensities. R. J. Kieber et al. (1997) found that photodegradation rates of C_{16} and C_{18} PUFA were nearly 10 times those of the species' monounsaturated counterparts; almost no photodegradation was observed in the saturated member of the C_{16} series, palmitic acid. Rontani et al. (1998) observed a similar trend for a series of $C_{18:1}$-$C_{18:3}$ fatty acids isolated from algal cultures; while that experiment did not include any PUFA with more than three double bonds, the degradation rate constant the authors observed for the $C_{18:3}$ species was more than six times that observed for $C_{18:1}$.

4.2.   Biogeochemical significance of lipid photooxidation in surface waters of the West Antarctic Peninsula

Our daily rate estimates of photooxidation of intact IP-DAG (Fig. 9) suggest the process is of a magnitude comparable to ecosystem bacterial production, making it a biogeochemically relevant pathway for the remineralization of particulate carbon in sunlit surface waters of the West Antarctic Peninsula. While limiting the scope of our findings to the early spring — when nearly all of the suspended particulate biomass in the shallow mixed layer receives enhanced doses of UVR through a depleted stratospheric ozone layer — we estimate conservatively that, on average, 0.7 ± 0.2 μmol IP-DAG m^{-2} d^{-1} was oxidized in the mixed layer by photochemical processes (using the conversion factor described in Section A.8 of the Appendix, this is the equivalent of 0.5 ± 0.1 mg C m^{-2} d^{-1}; Fig. 9, red markers and solid red trace). Under the second, less conservative scenario — in which we applied the AQY to a larger subset of the surface IP-DAG inventory — we estimate that approximately 6 times this quantity of lipid organic matter was potentially oxidized by sunlight (3.9 ± 1.1 μmol IP-DAG m^{-2} d^{-1}, equivalent to 2.7 ± 0.8 mg C m^{-2} d^{-1}; Fig. 9, cyan markers and dashed trace). For comparison, the mean mixed layer rates of bacterial production in the period before 4 January 2014 were 2.3 ± 1.8, 18.1 ± 17.2, and 14.4 ± 9.9 mg C m^{-2} d^{-1} in vicinity of the Palmer Station seawater intake, at PAL-LTER Station B, and at PAL-LTER Station E, respectively (Fig. 9, larger symbols; mean ± SD; n = 3, 5, and 3, respectively; the mean rates of

leucine incorporation in surface samples at stations B and E were 37 ± 28 and 37 ± 36 pmol L^{-1} hr^{-1}, respectively).

The rate of lipid photooxidation thus represented between 4.4 % (conservative scenario) and 24.5 % (alternative scenario) of the mean bacterial production rate measured in the WAP mixed layer during the austral spring (range in conservative scenario, 3-21 %; range in alternative scenario, 15-116 %; Fig. 9). We suspect that even our less conservative calculations might still represent an underestimate of the overall significance of lipid photooxidation in WAP waters because we did not apply our model to any fraction of the lipid biomass allocated to triacylglycerols, which accounted for 70-75 % of the total identifiable chromatographic peak area in the water column samples. Although the AQY was derived from photooxidation experiments with PC, we justify its application to other classes of IP-DAG on the basis of evidence (from human systems) that changes in headgroup do not dramatically affect *in situ* oxidation rates so long as the attached PUFA are of high unsaturation (Reis and Spickett, 2012). We also assumed in our calculations that the residence times of suspended and slowly sinking particulate organic matter in the mixed layer were long (i.e., on timescales of days) compared with the timescale over which photodegradation was observed to act in our liposome experiments (i.e., 8.2-12.4 hr).

4.3. Role and activity of heterotrophic bacteria

4.3.1. *Evidence for direct bacterial metabolism of unoxidized lipids*

We found only mixed evidence to support our hypothesis that bacteria would directly degrade the liposomes as a growth substrate. While we observed a small marginal enhancement in the apparent degradation rate of PC 22:6, 22:6 liposomes in the + UVR treatment when heterotrophic bacteria were present, this increase was not statistically significant (Fig. 3a; Table 1). We did observe some enhancement at the final timepoint in the hydrolysis of 4-methylumbelliferone-butyrate-heptanoate-palmitate (4-MUF-butyrate, monitored as a proxy for lipase activity) in the + UVR + het. bact. treatment compared with the dark control, suggesting at least some fraction of the bacterial community was attempting to metabolize the added lipids (Tukey HSD test with α = 0.05; Table A4). No significant

differences were observed between treatments in the hydrolysis of L-Leucine-4-methylcoumaryl-7-amide (leu-MCA, monitored for aminopeptidase activity; Table A4). That we did not find more conclusive evidence for bacterial degradation of the liposomes might have reflected widespread inhibition of the bacterial community by exposure to high doses of UVR during the experiments (Santos et al., 2011; Ward et al., 2017).

4.3.2.   Support for bacterial metabolism of oxidized degradation products

We found indirect evidence to support the related hypothesis that photooxidation could degrade intact lipids into smaller, more labile components that were amenable to microbial metabolism. For example, in comparing the + UVR - het. bact. treatment to the corresponding + UVR + het. bact. treatment, we noted greater net production in the former of nearly all the PC 22:6, 22:6 degradation products that we could identify in our HPLC-MS data (compare rightmost two columns in Fig. 4). One possible interpretation of these results is that some fraction of the oxidized compounds produced in the + UVR + het. bact. treatment was removed via heterotrophic metabolism. This interpretation is challenged by recent work showing heterotrophic bacteria cannot use oxylipins such as polyunsaturated aldehydes (PUA) — the highly bioactive derivatives of fatty acids that are considered the "terminal" products of lipid peroxidation — as a viable carbon source (Edwards et al., 2015; Ribalet et al., 2008). However, these studies did not evaluate the ability of heterotrophic bacteria to metabolize any of the many other compounds, such as LPC or intact ox-PC species, which we show were produced as intermediates in the course of photooxidation (Fig. 4).

4.4.   Possible mechanisms supporting observed rates of photooxidation

While the original scope of this work did not extend to identification of the mechanism(s) responsible for the photooxidation in our experiments or WAP waters generally, several conclusions can be drawn from synthesis of available data and previous findings regarding photochemical processes. Lipid photooxidation can be effected by one of three mechanisms: Type I (i.e., radical-mediated) sensitization, Type II (i.e., singlet oxygen-mediated) sensitization, and direct initiation by UVR; Girotti (1990) and

Schaich (2005) both include detailed schematics that illustrate the oxidation of lipids via these different pathways. Below, we briefly address the potential for each of these to have contributed to rates of photooxidation in our experimental system and, by comparison, in the surrounding environment. We ultimately conclude that the photooxidation in our experiments was a result of Type I processes, with likely additional contributions from (1) direct initiation by ultraviolet radiation and (2) light-dependent autoxidative processes that were not accounted for by our use of dark controls.

4.4.1. *Type I (radical-mediated) photooxidation*

The preferential removal of PC 22:6, 22:6 (compared with lipids containing more saturated acyl moieties; Table A1) suggested that at least some of the oxidation we observed in our experiments could have been attributed to a Type I mechanism. The particular vulnerability of *bis*-allylic hydrogen atoms in PUFA to abstraction by free radicals and the attendant relationship between acyl unsaturation and radical reactivity have been well-established (Cosgrove et al., 1987; Schaich, 2005; Wagner et al., 1994). While we did not monitor the production of radical species in our liposome experiments or in the waters surrounding Palmer Station, elevated production of hydroxyl radical from UVB photolysis of nitrate has been observed in WAP waters under ozone hole conditions similar to those observed in 2013 (D. J. Kieber et al., 2007; Qian et al., 2001; compare Fig. 2). Surface concentrations of NO_3^- + NO_2^- remained at or above 15 μM at PAL-LTER Stations B and E until early January (Kim et al., 2016), providing a sufficient reservoir of NO_x to sustain •OH production at biogeochemically significant rates. However, there is some evidence (Patterson and Hasegawa, 1978, as cited in Schaich, 2005) that •OH abstract acyl H atoms nonspecifically, showing no clear preference for the *bis*-allylic H atoms in PUFA. One might thus conclude •OH could not have been the primary initiator of peroxidation in the liposome experiments; according to this logic, we should not have seen such strong evidence for preferential oxidation if •OH were responsible. While this argues strongly against a primary role for hydroxyl radical, it does not preclude the more likely scenario in which long radical chain reactions were initiated by •OH but propagated by secondary lipid radicals such as LO• or LOO•, the latter of which do exhibit a clear

preference for *bis*-allylic H atoms (Cosgrove et al., 1987). Because it is these subsequent reactions that effect the vast majority of the lipid oxidation observed in Type I photochemistry (Girotti, 1990; Girotti, 2001; Schaich, 2005), we ultimately concluded that our results were consistent with the signature of a Type I mechanism. A Type I mechanism was also proposed for the *in situ* production of ω-oxocarboxylic acids from a monounsaturated C_{18} fatty acid in marine aerosols (Kawamura and Gagosian, 1987).

4.4.2. *Type II (singlet oxygen-photosensitized) photooxidation*

In contrast, we found it unlikely Type II photochemical processes could have contributed to the oxidation we observed in our experimental system, chiefly because the lack of photosensitizers such as chlorophyll would not have supported production of singlet oxygen in the liposome suspensions. Type II photooxidation of lipids has been proposed as the dominant pathway in marine systems for photooxidation of monounsaturated fatty acids and photosynthetic pigments in marine detritus (Nelson, 1993; Rontani, 1999, 2001; Rontani et al., 2016), and liposomes such as those we employed in our experiments create precisely the sort of "hydrophobic microenvironment" that can extend the lifetime and steady-state concentrations of singlet oxygen well beyond the bulk aqueous phase (Latch and McNeill, 2006). Because conditions in Arthur Harbor almost certainly would have supported production of singlet oxygen in these sorts of microenvironments, particularly in detritus from senescent ice-attached algal communities, the absence of Type II processes from the experimental system upon which we based our AQY calculations is cause to presume our model results (Fig. 9) may represent a sizeable underestimate of true photooxidation rates in the environment. We believe our model results may further underestimate true rates of photooxidation for a related reason: We confined ourselves to calculations based solely on UV radiation, which is attenuated much more rapidly in the water column than the visible light that catalyzes Type II processes.

4.4.3. *Direct initiation by UVR*

Finally, we conclude that direct initiation by UVR could have augmented Type I radical-mediated processes in our both our experiments and the environment. Direct initiation of lipid oxidation

by UVR requires that the photon energy available in incoming light meet or exceed the energy required for bond scission in the molecule of interest (Schaich, 2005), and that the molecule be capable of absorbing light at the wavelength(s) corresponding to the minimum actionable photon energy. Light was not limiting in our experiments or the surrounding environment: We measured ample photons of wavelength ≥ 320 nm within the aquarium and in the water column to depths of 8 m (Fig. A3; see also results presented in Section 3.1). In addition, our laboratory spectrophotometer measurements indicated that the DHA-containing IP-DAG PC 22:6, 22:6 absorbs light very strongly throughout the UVB spectrum and well into the UVA (log ε_i ≥ 1 M^{-1} cm^{-1} at wavelengths as long as 340 nm; Fig A4c). Concurrent measurements of DHA, the constituent fatty acid of PC 22:6, 22:6, indicated that the parent molecule's light-absorbing capacity was due primarily to the presence of the highly unsaturated acyl moiety and not the polar headgroup (Fig. A4b,c). Finally, the 314-335 kJ mol^{-1} bond energy previously reported for the doubly allylic C-H bonds in model PUFA (Gardner, 1989; Koppenol, 1990) is equivalent to that carried by UVA-band photons of λ between 357 and 381 nm, which were abundant at the 0.6 m depth of our experimental system and throughout the water column in the surrounding environment. However, there is strong evidence that the favorable thermodynamics of these reactions may be alone insufficient to support direct initiation. Schaich (2005), for example, reported activation energies for such bond scission reactions of at least 471 kJ mol^{-1}, equivalent to photon energy at 254 nm; light of this wavelength is rarely available at the earth's surface, even during ozone hole events in Antarctica. Therefore, while it is possible direct initiation by UVR could have augmented Type I photooxidative processes in both our experimental system and the surrounding environment, we conclude that any contribution would have been minor given the high reported activation energies.

4.5. Future implications for the West Antarctic Peninsula marine ecosystem

Three major, relatively recent changes in the ecosystem of the WAP (Ducklow et al., 2013; Saba et al., 2014) make it difficult to predict how (or whether) lipid photooxidation will impact rates of

primary production or carbon export in the future. First, shifts in the diversity of the phytoplankton community responsible for primary production in waters of the WAP will likely drive shifts in the lipid composition of surface ocean biomass during and after the annual retreat of the sea ice. Among these shifts in community composition is an increase the prevalence of cryptophytes, a clade of poorly understood algae of class Cryptophyceae, at the expense of the diatoms traditionally responsible for most of the carbon fixation in WAP waters (Montes-Hugo et al., 2009; Schofield et al., 2017). The stark differences between our water column lipid profiles (Fig. 7) and those of four diatoms isolated during the same season (Fig. A9) suggests taxa other than diatoms are already contributing in great numbers to the surface ocean particulate lipid reservoir. Microscope observations of water samples collected in 2013 and 2014 confirmed that cryptophytes were present in WAP waters in large numbers (data not shown). Relatively little is known about the lipids of cryptophytes apart from a few instances in which the species have been investigated for their potential as a feedstock for biodiesel production (Henderson and Mackinlay, 1989).

Second, should the rapid warming of WAP waters that has been observed in recent decades continue (Ducklow et al., 2013), the increase in average sea surface temperature could drive changes in the saturation state of the marine lipid pool independent of any change attributable to shifts in species distribution. Experimental results in cultures of several different marine phytoplankton show that even modest increases in temperature can drive measureable decreases in the proportion of overall membrane lipids that contain polyunsaturated fatty acids (Guschina and Harwood, 2006). This general relationship between saturation state and temperature has been demonstrated specifically in cultures of *Chroomonas salina* (Henderson and Mackinlay, 1989). While the lipid inventories at several sites along the WAP presently include robust concentrations of IP-DAG with sufficient PUFA to support biogeochemically significant rates of photooxidation (Fig. 8, Fig. 9), warmer waters and an ecological shift toward phytoplankton species of largely uncharacterized lipid composition could alter the significance of photooxidation in the ecosystem.

Third, reductions in the duration and extent of sea ice cover that have accompanied the increase in WAP sea surface temperatures (Meredith and King, 2005) will likely diminish the strength of ice-associated and ice-attached diatom communities and their relative contribution to the overall lipid pool. The membrane lipids produced by ice-attached diatom communities can differ in fatty acid chain length, saturation state, and even lipid class distribution from those produced by planktonic diatoms (Fahl and Kattner, 1993; Falk-Petersen et al., 1998; Mock and Kroon, 2002). Because primary production in WAP waters is typically distinguished by bloom events that begin at the receding sea ice edge in spring or early summer (Ducklow et al., 2013; Kim and Ducklow, 2016; Vernet et al., 2008), warming water and concomitant changes in annual sea-ice dynamics could also advance the timing of blooms to earlier in spring and shift their locations further south, which could lead to ever greater temporal and spatial coincidence between maximum UVR exposure and peak phytoplankton abundances. A final, more recent trend — the reduction in the size of and severity of the seasonal ozone (O_3) anomaly over Antarctica, driven by recovery in stratospheric O_3 stocks (Solomon et al., 2016) — could represent an important negative feedback on photooxidation, further complicating any attempt to predict the overall significance of the process in a future ecosystem state.

5. Conclusions

We show here that photooxidation of lipids containing polyunsaturated fatty acids is a relevant pathway for carbon turnover in the surface ocean on scales commensurate with bacterial production. Our results suggest that the shallow mixed layers that can form in the marginal ice zone provide a sort of "optical incubator" for UVR-induced lipid peroxidation in the WAP. In this model, particulate organic matter, including both ice-attached and free-living phytoplankton and bacteria, is exposed for extended periods to intense UV radiation at the immediate sea surface, increasing photooxidation rates of photolabile compounds such as PUFA-containing IP-DAG. Deployment of sediment traps during future studies would allow us to determine whether these PUFA-derived ox-IPL and oxylipins leave a significant imprint on the organic matter exported to the ocean's depths, as evidence suggests is true of

MUFA-derived oxylipins from photochemical processes (Marchand and Rontani, 2001; Rontani, 1999; Rontani et al., 2016; Rontani et al., 2012a; Rontani et al., 2012b).

The pairing of a high-resolution, accurate-mass HPLC-ESI-MS method with an enhanced lipidomics discovery strategy allowed us to build a comprehensive profile of the lipids of West Antarctica's marine microbial community. Future studies will be needed to determine the relative contributions of Type I, Type II, and direct photolysis mechanisms to overall rates of lipid photooxidation in Antarctic surface waters. Apart from the use of traditional photochemical probes, direct insight might be gained through further structural elucidation of the many oxidized lipids identified in experiments such as those we present in this work (e.g., Fig. 4, Fig. 5). Additional in-source fragmentation of target analytes, combined with some derivatization prior to analysis, may be necessary to localize the oxidized functional groups on a given molecule.

Finally, while we documented the abiotic production of a diversity of oxidized phospholipids under natural conditions in the environment, this study did not address the many possible infochemical impacts that these new compounds might have on intracellular processes, interactions between microoorganisms in the water column, or on the remineralization of sinking marine particles. Given the hundreds of other oxylipins and many different intact oxidized phospholipids with significant known or hypothesized bioactivities in humans and terrestrial plants, it is highly probable that some of these same compounds or their close analogs must play similar or as-yet-unimagined roles in the ocean.
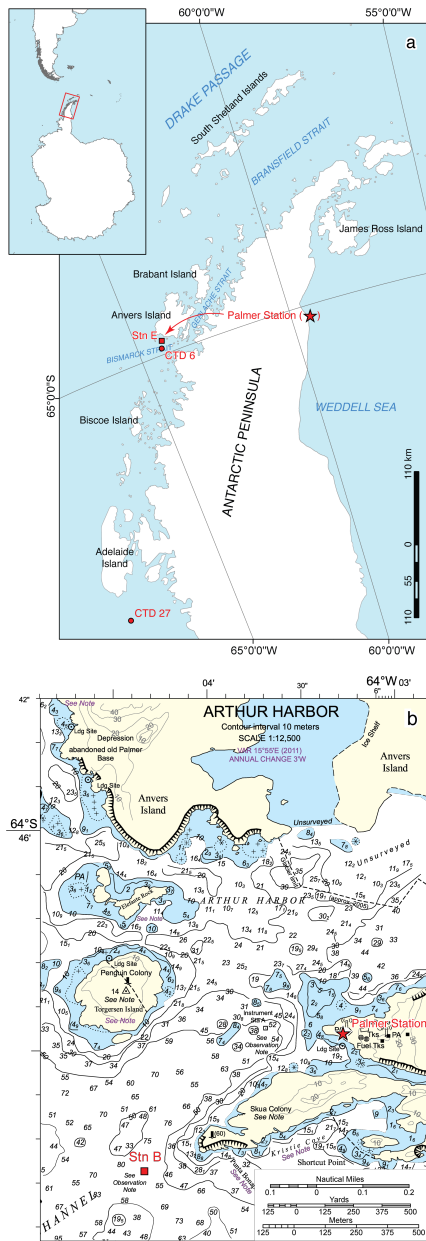
6.   Acknowledgements

Figures

Fig. 1. (a) Map of the West Antarctic Peninsula, showing locations of sampling stations referenced in the text (Palmer Long Term Ecological Research study station E, ■; CTD casts 6 and 27 during cruse LMG 14-01, ◉) and of Palmer Station (★). Inset shows extent of map view in relation to Antarctica and South America. (b) Detail from U.S. National Geospatial Intelligence Agency (NGA) nautical chart 29123 (INT 9105), showing bathymetry and major marine features in immediate vicinity of Palmer Station.
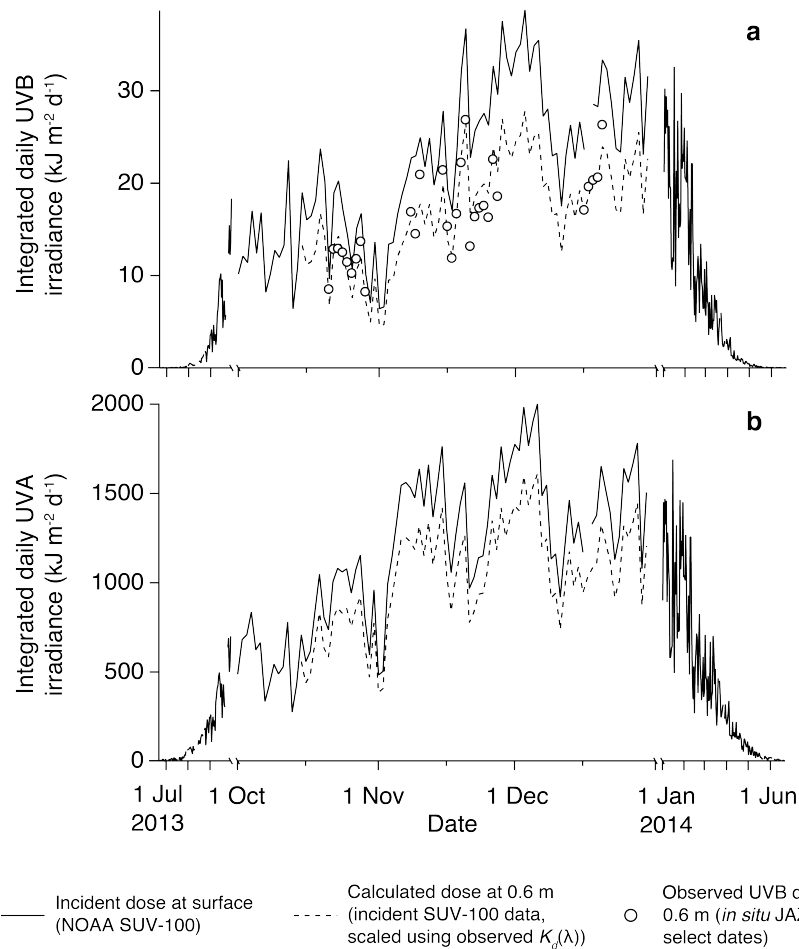
Fig. 2. Time- and wavelength-integrated daily doses of (a) UVB (290-315 nm) and (b) UVA (315-400 nm) radiation received at Palmer Station from 1 July 2013 to 30 June 2014. Solid traces: Incident doses at the ocean surface from SUV-100 spectroradiometer data (courtesy U.S. National Oceanic and Atmospheric Administration (NOAA) Antarctic UV Monitoring Network, NOAA Global Monitoring Division, Boulder, CO, USA). Dashed traces (sections with expanded *x*-axis): Estimated downwelling doses of UVB and UVA radiation at 0.6 m water depth, calculated according to Eqs. A.1-A.3 from incident SUV-100 data and $K_d(\lambda)$ obtained from water column profiles (Fig. A3). Open circles (select dates): Daily UVB doses at 0.6 m from *in situ* measurements with a calibrated Ocean Optics Jaz spectrometer, as described in the text. The largest daily dose of UVB radiation was received on 3 December 2013 even though the seasonal minimum in total column ozone (154.82 Dobson units) was recorded on 12 October 2013.
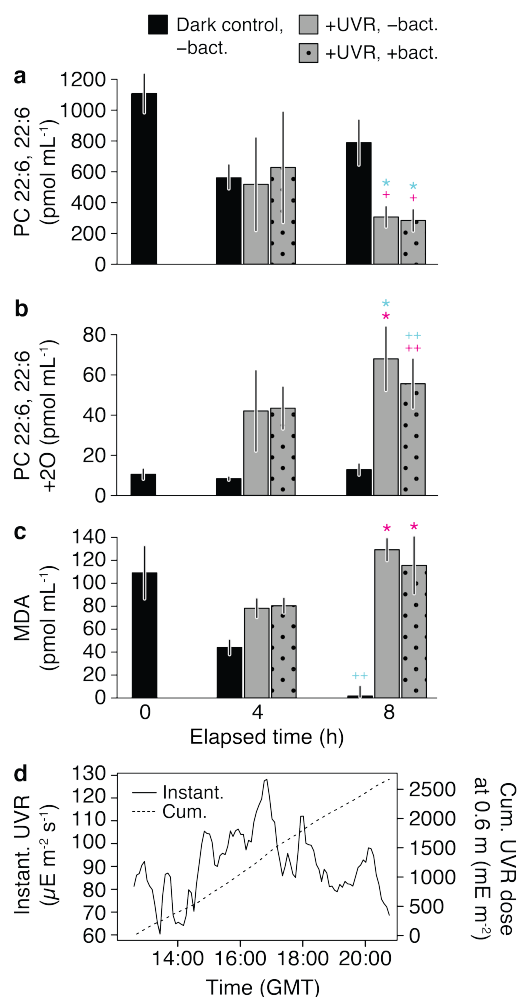
Fig. 3. Results from a lipid photooxidation experiment conducted with phosphatidylcholine (PC) liposomes at Palmer Station on 14 December 2013. Concentrations after 4 and 8 h of (a) PC 22:6, 22:6, (b) an intact oxidation product (PC 22:6, 22:6 +2O; identified at chromatographic retention time 10.4 min.), and (c) malondialdehyde, a commonly-used indicator of lipid peroxidation activity. Error bars: ± SE of mean (initial concentrations, n = 4 replicates; all other treatments and time points, n = 3). Symbols in (a)-(c) indicate significance of difference of mean from initial dark control (cyan symbols) or difference from dark control at final timepoint (magenta symbols) according to Tukey's Honest Significant Difference method with α = 0.05: $p ≤ 0.1$ (+), $p ≤ 0.05$ (++), $p ≤ 0.01$ (*). (d) Instantaneous (solid line) and cumulative (dashed line) downwelling UVR photon fluxes (290-400 nm) measured at the incubation depth using an *in situ* spectrophotometer (0.6 m).
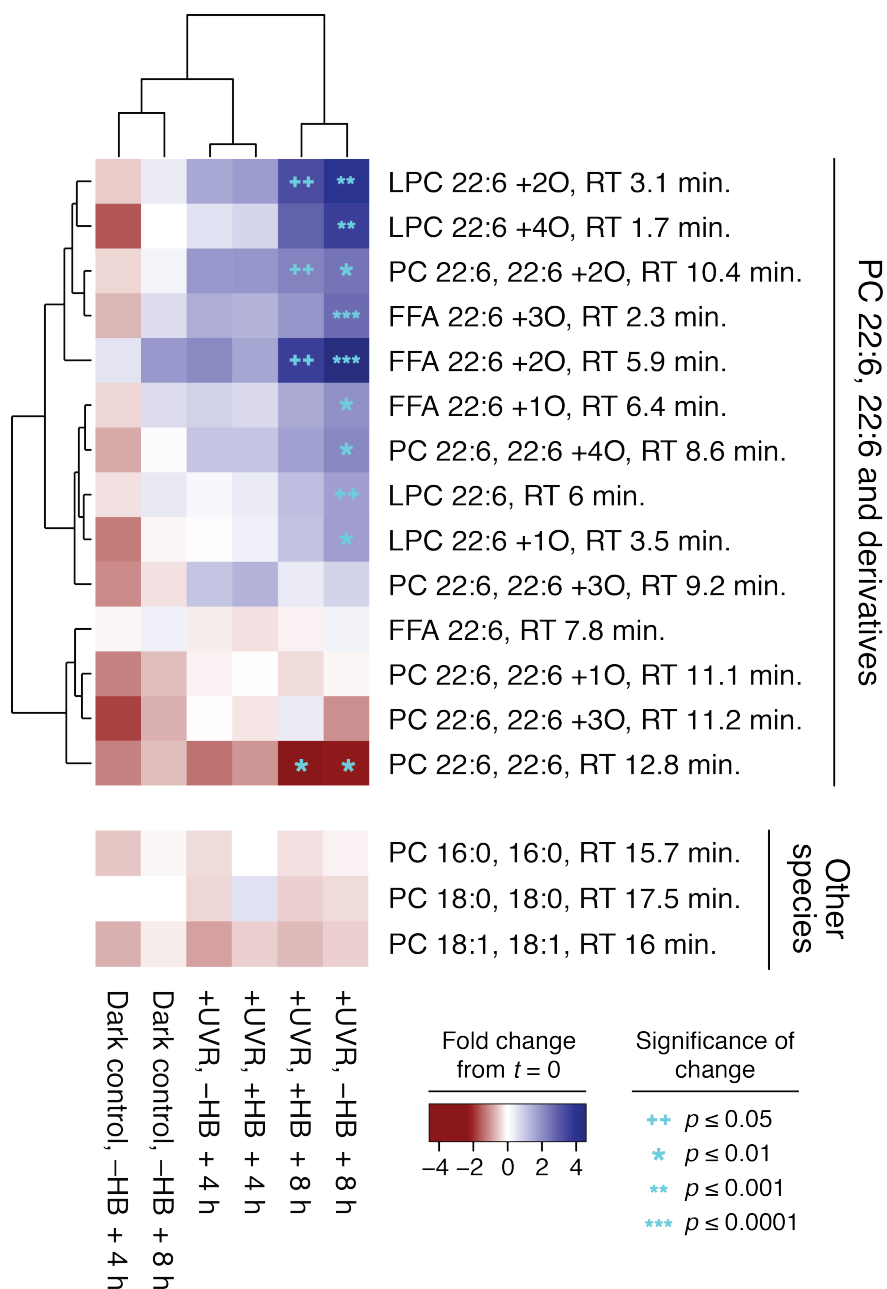
30

Fig. 4. Changes in the concentration of PC 22:6, 22:6 and various molecular derivatives during the liposome photooxidation experiment presented in Fig. 3. For a given treatment and timepoint on the *x*-axis, cell color shows the fold change in concentration of each molecule on the *y*-axis relative to the concentration observed at the initial experimental timepoint. Fold-change calculations are based on mean concentrations measured at each treatment and time point in at least 3 replicates. The order of both rows (analytes) and columns (treatment-time point combinations) reflects application of an unsupervised

clustering algorithm (function "hclust," part of the R stats package). The dendrogram shows similarity (by Euclidean distance) among analytes and treatments/time points. Symbols in cyan indicate the statistical significance of the difference of each mean concentration relative to the mean concentration at the initial time point according to Tukey's "Honest Significant Difference" method with $\alpha = 0.05$: $p \leq 0.05$ (++), $p \leq 0.01$ (*), $p \leq 0.001$ (**), $p \leq 0.0001$ (***). The lower subplot shows changes in concentration observed in the other PC species evaluated in the same experiment; no significant changes were observed in any of the species containing fully saturated or monounsaturated fatty acids. The heatmap was generated in R (R Core Team, 2016) using the gplots (Warnes et al., 2016) package.
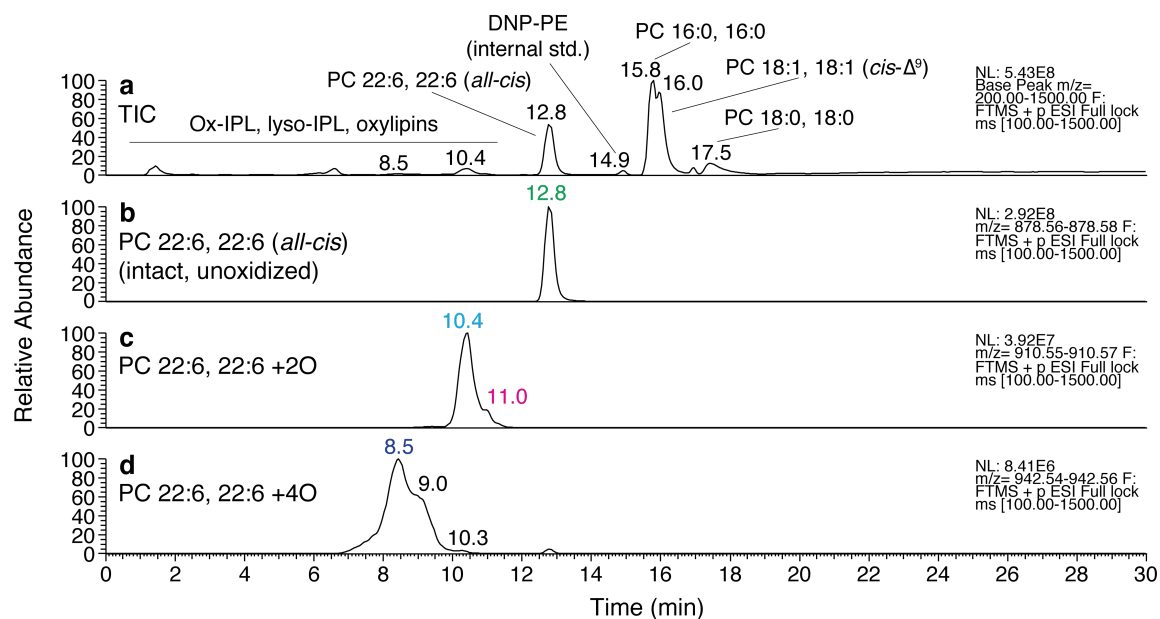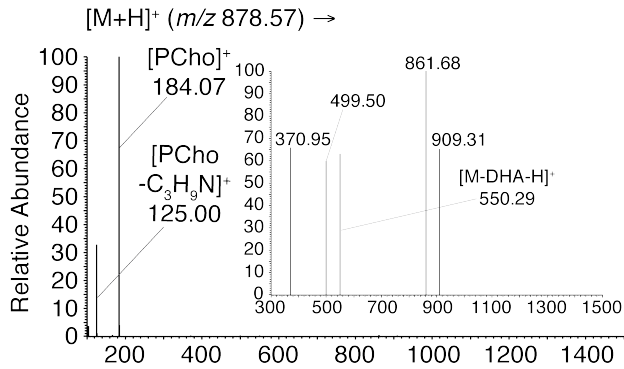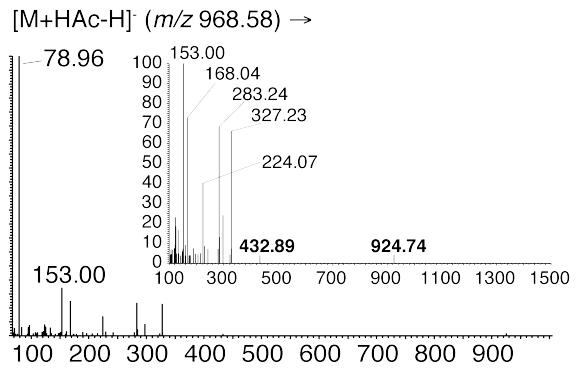
Fig. 5. Lipids and oxidized lipids identified in a lipid photooxidation experiment on 14 December 2013. (a) Total ion chromatogram showing all lipids identified in one of three replicate samples of the + UVR - het. bact. treatment at the final experimental time point (8 h) shown in Fig. 3. (b)-(d) Extracted ion chromatograms showing the unoxidized PC 22:6, 22:6 parent molecule and two intact oxidized degradation products (ox-PC). Major features are identified by retention time; colored annotations in (b)-(d) correspond to colors used in column headings in Fig. 6 and Fig. A7. Analysis of full-scan and dd-MS^2 spectra corresponding chromatographically to the different shoulders of the compound peaks in (c) and (d) suggests multiple positional isomers of each species were present in the sample.

a PC 22:6, 22:6 (*all-cis*), RT 12.8 min.

[M+H]$^+$ (*m/z* 878.57) →

[PCho]$^+$ 184.07

[PCho -C$_3$H$_9$N]$^+$ 125.00

Relative Abundance

370.95   499.50   861.68   909.31
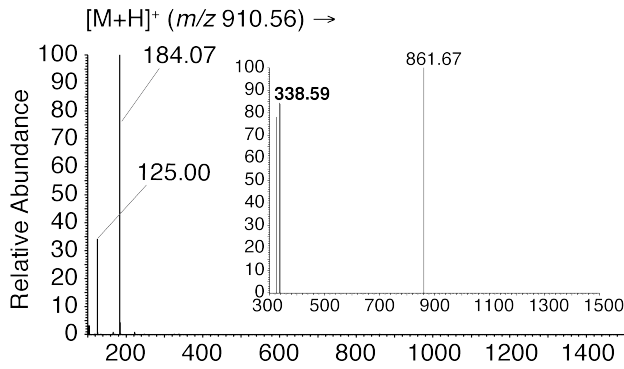
[M-DHA-H]$^+$ 550.29

[M+HAc-H]$^-$ (*m/z* 936.58) →

[PO$_3$]$^-$ 78.96

[DHA -CO$_2$]$^-$ 283.24

[DHA]$^-$ 327.23

[GlyPCho- CH$_3$-H$_2$O]$^-$ 224.07

[PCho -CH$_3$]$^-$ 168.04

[C$_{17}$H$_{25}$]$^-$ 229.20

[C$_3$H$_6$O$_5$P]$^-$ 153.00

b PC 22:6, 22:6 +2O, RT 10.4 min.

[M+H]$^+$ (*m/z* 910.56) →

184.07

125.00

560.11
656.53

[M+HAc-H]$^-$ (*m/z* 968.58) →

78.96

153.00

153.00   168.04   283.24   327.23   224.07

432.89   **924.74**

c PC 22:6, 22:6 +2O, RT 11.0 min.

[M+H]$^+$ (*m/z* 910.56) →

184.07

125.00

338.59   861.67

[M+HAc-H]$^-$ (*m/z* 968.58) →

78.96

153.00

153.00   168.04   283.24   327.23   224.07

368.58   **887.44**   **943.51**
710.59

d PC 22:6, 22:6 +4O, RT 8.5 min.

[M+H]$^+$ (*m/z* 942.55) →

184.07

125.00

447.96   861.69
369.67

[M+HAc-H]$^-$ (*m/z* 1000.56) →

78.96

153.00

327.23   943.75

153.00   168.04   224.07   283.24   327.23
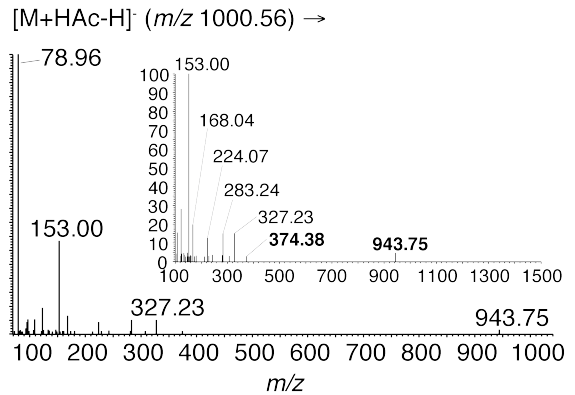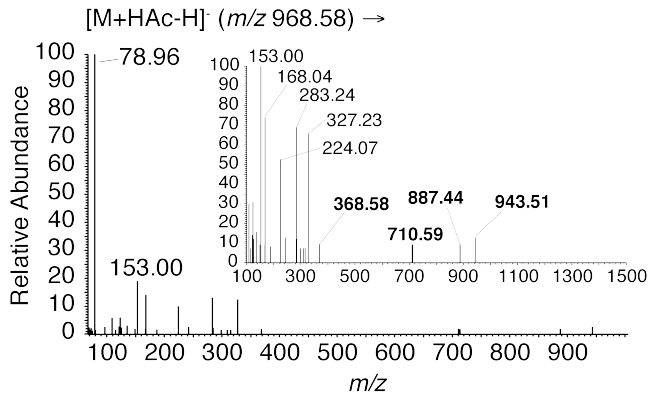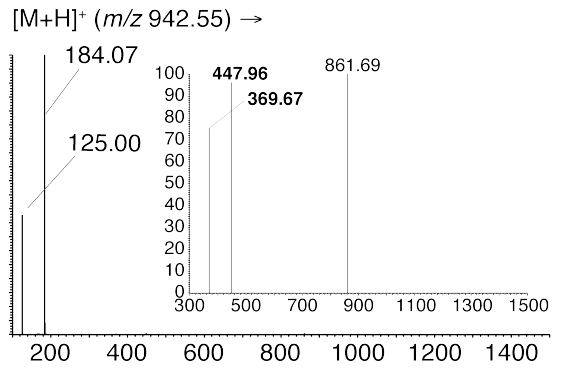
374.38   **943.75**

m/z

Fig. 6. Data-dependent MS^2 spectra of (a) PC 22:6, 22:6 and (b)-(d) the three oxidized degradation products identified in the + UVR - het. bact. sample presented in Fig. 5. The top and bottom plots in each subpanel show, respectively, the positive and negative ionization mode fragmentation spectra for the major adduct of each analyte. Labeled features in (a) are the major ions diagnostic of the intact, unoxidized parent molecule; some of these are diagnostic PC headgroup fragments that also appear in (b)-(d). Boldface *m/z* annotations in (b)-(d) indicate fragment ions unique to each oxidized species. Text colors used in column headings correspond to those used in Fig. 5 and Fig. A7. An expanded version of Fig. 6 is presented in Fig. A7.
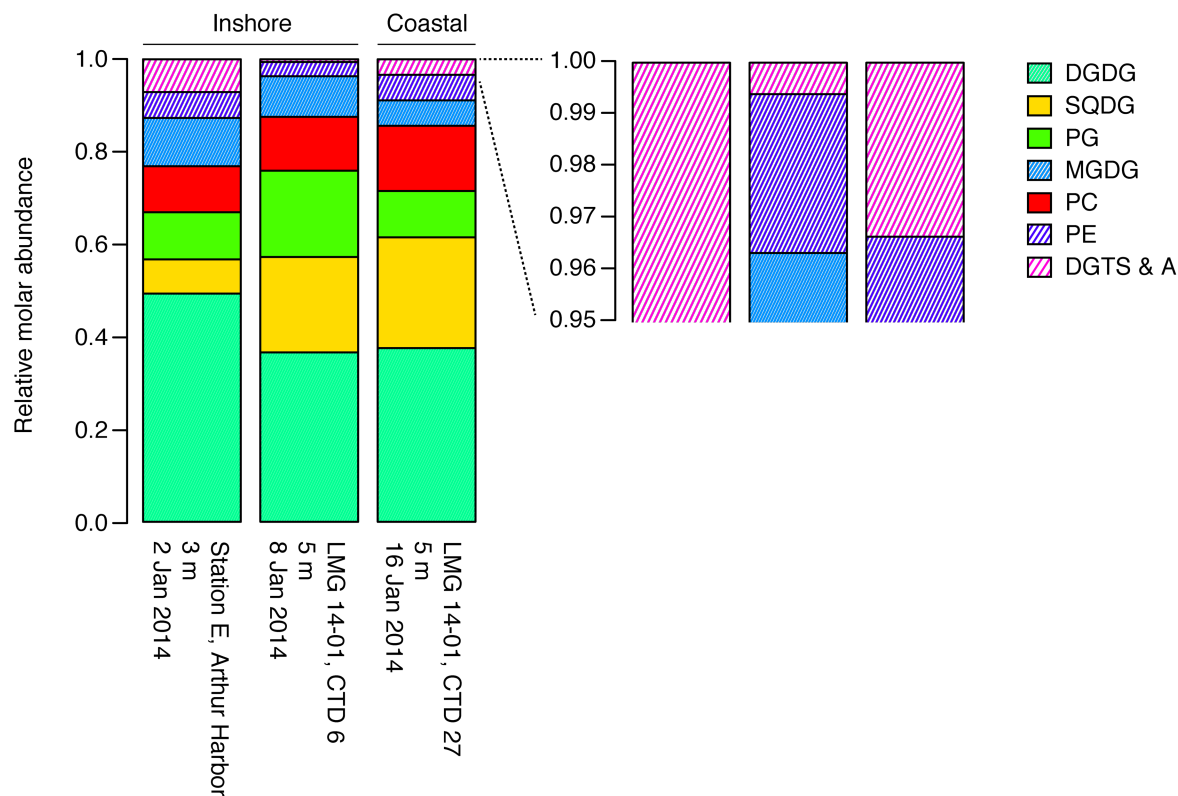
Fig. 7. Relative molar distribution of seven classes of intact polar diacylglycerol (IP-DAG) in representative samples of particulate biomass (fraction > 0.2 μm) from waters of the West Antarctic Peninsula. Samples were collected in 2014 from an inshore station (PAL-LTER Station E, 64.82° S, 064.055° W) and two coastal stations whose biogeochemistry was representative of oceanic influence (cruise LMG 14-01, CTDs 6 and 27, 64.88° S, 064.289° W, and 68.159° S, 068.946° W, respectively; Fig. 1). The CTD 6 (8 Jan) sample was obtained during a significant bloom event. Lipids were identified using the LOBSTAHS software (Collins et al., 2016) in conjunction with several additional criteria described in the text; 318 different compounds are represented in the figure. Quantification of lipids was performed using authentic standards. The full, annotated list of the lipids identified in each culture is available online at https://doi.org/10.5281/zenodo.841930 (version of record) or via direct download at https://github.com/jamesrco/LipidPhotoOxBox/blob/master/data/nice/LOBSTAHS_lipid_identities/PAL1314_LMG1401_particulate_IP-DAG_pmol_L.final.csv.

a All identifiable IP-DAG

b Phosphatidylcholine (PC) only
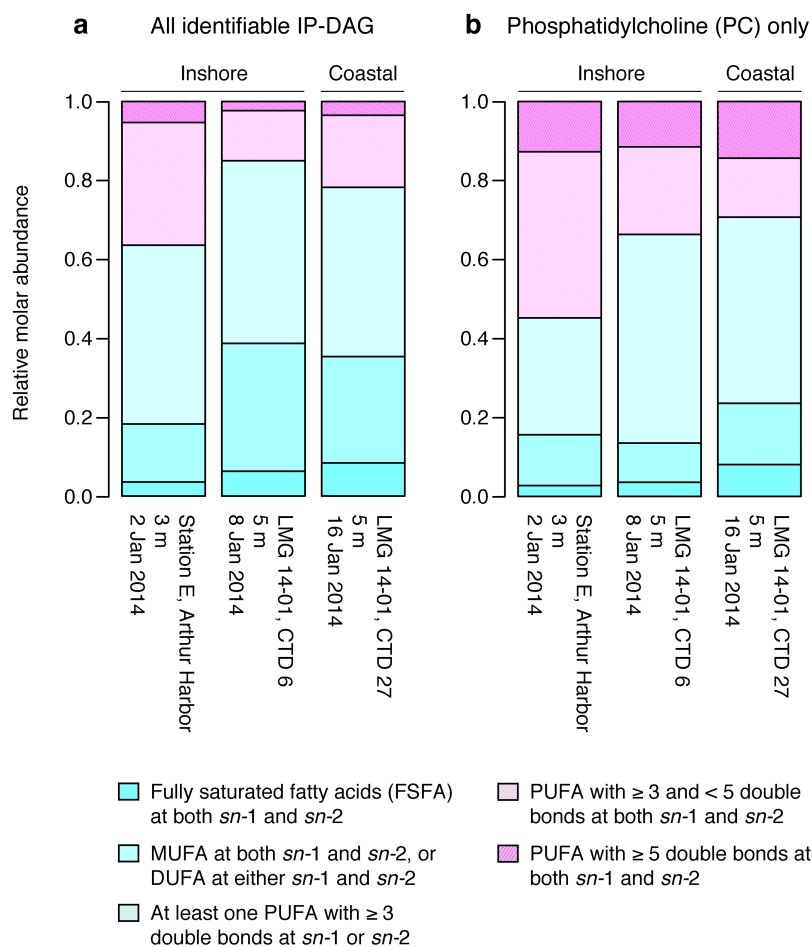
Fig. 8. Fatty acid composition of (a) all identifiable IP-DAG and (b) phosphatidylcholine (PC) species in the particulate biomass samples for which distributions of IP-DAG are presented in Fig. 7. Because the current version of the LOBSTAHS software resolves the identities of IP-DAG only to the level of bulk fatty acid composition (i.e., the sum of the properties of the substituents at both the *sn*-1 and *sn*-2 positions), we were unable to determine which fatty acids were present in each molecule without additional inspection of fragmentation spectra or saponification for analysis of fatty acid methyl esters (FAMES). However, we were able to categorize the saturation state of the IP-DAG according to the simplified scheme we present here after verifying (by inspection of fragmentation spectra) that the maximum degree of unsaturation of any single fatty acid present in these species was six (present in the form of docosahexaenoic acid, or DHA).
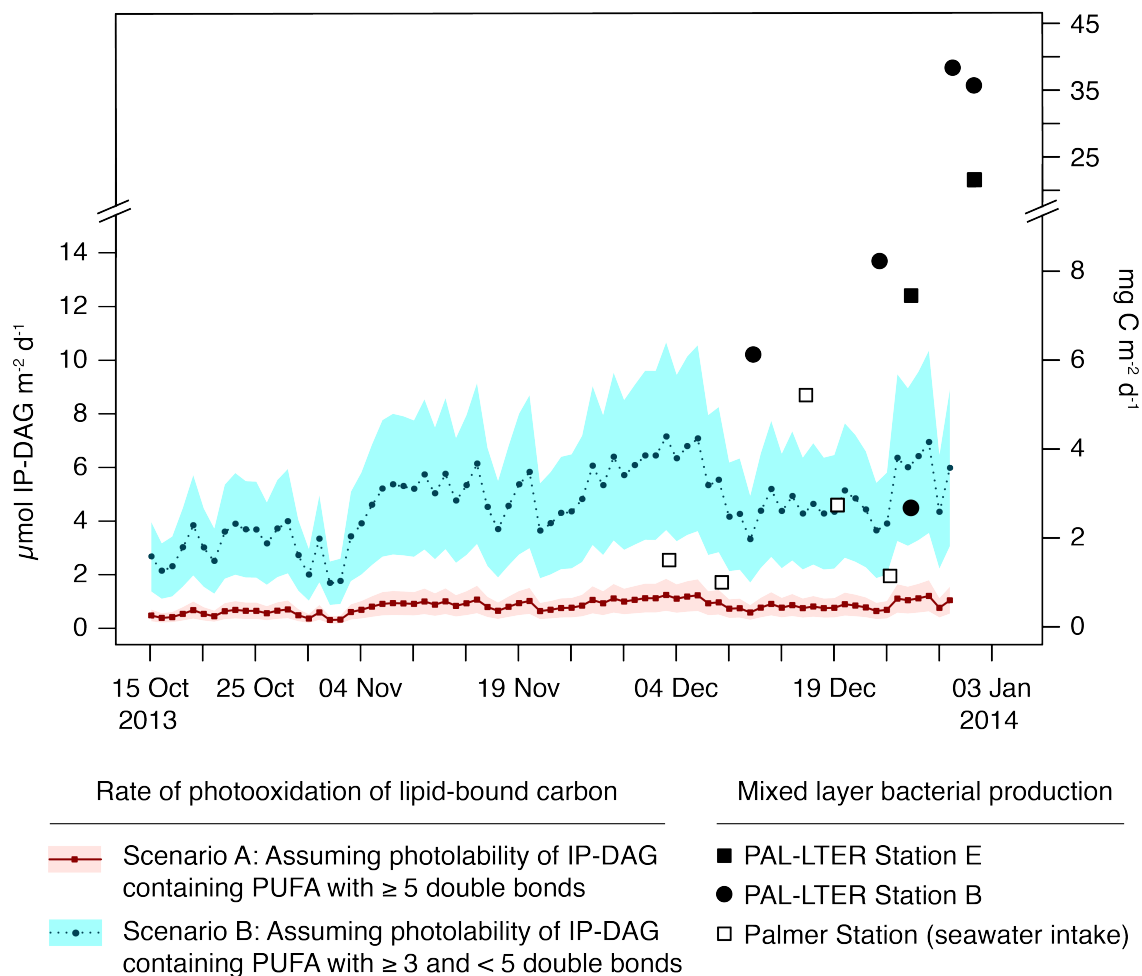
Fig. 9. Potential rates of lipid photooxidation in mixed layer waters of the West Antarctic Peninsula over a 2-month period in the austral spring of 2013. High-resolution time-series estimates of downwelling irradiance and a broadband apparent quantum yield (AQY) for IP-DAG species containing highly polyunsaturated fatty acids (Φ_{UVR}) were applied to separate fractions of lipids identified using the LOBSTAHS software to generate two sets of photooxidation rate estimates. In the first, most conservative scenario (red markers and solid trace), we applied the irradiance time series and AQY to only those IP-DAG containing PUFA with ≥ 5 double bonds at both the *sn*-1 and *sn*-2 backbone positions. In the second, more permissive scenario (cyan markers and dashed trace), we assumed the AQY could also be applied to molecular species containing PUFA with ≥ 3 but < 5 double bonds. Φ_{UVR} represents the reaction yield for lipid photooxidation based on the quantity of UV radiation received between 290 to

395.5 nm; estimation of Φ_{UVR} is described in Section 2.6 of the text. The shaded regions represented the propagated uncertainties in each estimate determined using a series of Monte Carlo simulations. Lipid photooxidation rates (left-hand y-axis) were converted to units of mg C m^{-2} d^{-1} based on the mean carbon content of the IP-DAG identified in each unsaturation fraction; these were 49. 3 ± 0.5 and 50.6 ± 0.6 mol C : mol lipid for the polyunsaturated (cyan) and highly polyunsaturated (red) fractions, respectively. Presented for comparison are depth-integrated rates of bacterial production measured in Arthur Harbor using the ^{3}H-leucine incorporation method (large individual symbols, from PAL-LTER data; Bowman et al., 2016). Note the break and change in scale of the y-axis.

Table 1

Fate of molecular species identified during UVR-induced oxidation of a PUFA-containing phospholipid.[a]

Molecular species	Corrected retention time (min.)	Observed m/z[b]	Calculated m/z[c]	Rel. mass uncertainty of database match (ppm)	Change in concentration[d] (pmol mL^{-1} ± SE)			
					Treatment			
					Control (dark) - het. bact.	Control (dark) + het. bact.	+ UVR - het. bact.[e]	+ UVR + het. bact.[f]
PC 22:6/22:6	12.8	878.5693	878.5694	0.1	-322 ± 229	-223 ± 307	**-804 ± 188***	**-827 ± 190***
PC 22:6/22:6 +1O	11.1	894.5647	894.5643	0.4	ns[g]	ns	ns	ns
PC 22:6/22:6 +2O	10.4	910.5595	910.5593	0.3	ns	ns	**58.7 ± 16.0***	**46.3 ± 12.5**
PC 22:6/22:6 +3O	9.2	926.5546	926.5542	0.5	ns	ns	ns	ns
PC 22:6/22:6 +4O	8.6	942.5493	942.5491	0.2	ns	ns	**24.0 ± 7.3***	ns
LPC[h] 22:6	6.0	626.3496	626.3463	5.2	ns	ns	**38.1 ± 12.8**	ns
LPC 22:6 +1O	3.5	626.3441	642.3413	4.5	ns	ns	**1.0 ± 0.3***	ns
LPC 22:6 +2O	3.1	658.3384	658.3362	3.4	ns	ns	**8.9 ± 2.2****	**5.2 ± 1.0**
LPC 22:6 +4O	1.7	690.3319	690.3260	8.6	ns	ns	**5.4 ± 1.5****	ns
DHA[i]	7.8	327.2328	327.2330	0.5	ns	ns	ns	ns
DHA +1O	6.4	343.2283	343.2279	1.2	ns	ns	**0.2 ± 0.05***	ns
DHA +2O	5.9	359.2231	359.2228	0.8	ns	ns	**0.4 ± 0.1*****	**0.2 ± 0.03**
DHA +3O	2.3	375.2180	375.2177	0.8	ns	ns	**0.06 ± 0.02*****	ns

[a] Experiment conducted on 14 Dec 2013; results from the other four liposome experiments are summarized in Table A1. Concentration data in this table may be normalized to light quantity by dividing by 2.55 E m^{-2}, the total number of photons between 290-400 nm received within each treatment vessel over the duration of the experiment (8.2 hr). This figure was obtained by correcting the incident UVR photon flux observed *in situ* at 0.6 m (2.67 E m^{-2}) for the reduction in transmission by the quartz vessel wall (Fig. A1).

[b] Mean m/z of features in peak group to which this compound assignment was made. PC 22:6/22:6 and derivative ox-PC species were identified in positive ionization mode as [M+H]$^+$ adducts; LPC and ox-LPC were identified in negative ion mode as [M+HAc-H]$^-$ adducts; DHA and oxidized derivatives were identified in negative ion mode as [M-H]$^-$ adducts.

[c] For PC 22:6/22:6 and ox-PC species, m/z of [M+H]$^+$ adduct; for DHA and derivatives, m/z of [M-H]$^-$ adduct; for LPC and derivatives, m/z of [M+HAc-H]$^-$ adduct.

[d] For other than the intact parent molecule (PC 22:6, 22:6), changes are reported only where mean final concentration was significantly different from mean initial concentration according to Tukey's Honest Significant Difference method with α = 0.05: $p ≤ 0.05$ (**bold**), $p ≤ 0.01$ (*), $p ≤ 0.001$ (**), p ≤ 0.0001 (***); rates are reported as mean ± SE of results in n ≥ 3 replicates.

[e] 0.2 µm filtered seawater matrix

[f] 0.7 µm filtered seawater matrix

[g] ns: not significant

[h] LPC: lysophosphatidylcholine

[i] DHA: docosahexaenoic acid, 22:6(n-3)

References

Amiraux, R., Belt, S.T., Vaultier, F., Galindo, V., Gosselin, M., Bonin, P. and Rontani, J.-F. (2017) Monitoring photo-oxidative and salinity-induced bacterial stress in the Canadian Arctic using specific lipid tracers. *Mar. Chem.* **194**, 89-99.

Andreou, A. and Feussner, I. (2009) Lipoxygenases - Structure and reaction mechanism. *Phytochemistry* **70**, 1504-1510.

Armstrong, D. and Browne, R. (1994) The analysis of free radicals, lipid peroxides, antioxidant enzymes and compounds related to oxidative stress as applied to the clinical chemistry laboratory. In *Free Radicals in Diagnostic Medicine: A Systems Approach to Laboratory Technology, Clinical Correlations, and Antioxidant Therapy* (ed. D. Armstrong). Springer US, Boston, MA. pp. 43-58.

Barofsky, A. and Pohnert, G. (2007) Biosynthesis of polyunsaturated short chain aldehydes in the diatom *Thalassiosira rotula*. *Org. Lett.* **9**, 1017-1020.

Benton, H.P., Want, E.J. and Ebbels, T.M.D. (2010) Correction of mass calibration gaps in liquid chromatography-mass spectrometry metabolomics data. *Bioinformatics* **26**, 2488-2489.

Bernhard, G., Booth, C.R. and Ehramjian, J.C. (2005) UV climatology at Palmer Station, Antarctica, based on Version 2 NSF network data, In *Ultraviolet Ground- and Space-based Measurements, Models, and Effects V, 588607* (eds. G. Bernhard, J.R. Slusser, J.R. Herman and W. Gao). Proc. SPIE Int. Soc. Opt. Eng. pp. 588607-01-588607-12.

Bernhard, G., Booth, C.R. and Ehramjian, J.C. (2010) Climatology of ultraviolet radiation at high latitudes derived from measurements of the National Science Foundation's Ultraviolet Spectral Irradiance Monitoring Network. In *UV Radiation in Global Climate Change: Measurements, Modeling and Effects on Ecosystems* (eds. W. Gao, J.R. Slusser and D.L. Schmoldt). Springer Berlin Heidelberg, Berlin. pp. 48-72.

Biavati, G. (2014) RAtmosphere: Standard amospheric profiles. R package, version 1.1.

Bligh, E.G. and Dyer, W.J. (1959) A rapid method of total lipid extraction and purification. *Canadian Journal of Biochemistry and Physiology* **37**, 911-917.

Bowman, J.S., Vick-Majors, T.J., Morgan-Kiss, R., Takacs-Vesbach, C., Ducklow, H.W. and Priscu, J.C. (2016) Microbial community dynamics in two polar extremes: The lakes of the McMurdo Dry Valleys and the West Antarctic Peninsula marine ecosystem. *Bioscience* **66**, 829-847.

Brash, A.R. (1999) Lipoxygenases: Occurrence, functions, catalysis, and acquisition of substrate. *J. Biol. Chem.* **274**, 23679-23682.

Buseman, C.M., Tamura, P., Sparks, A.A., Baughman, E.J., Maatta, S., Zhao, J., Roth, M.R., Esch, S.W., Shah, J., Williams, T.D. and Welti, R. (2006) Wounding stimulates the accumulation of glycerolipids containing oxophytodienoic acid and dinor-oxophytodienoic acid in *Arabidopsis* leaves. *Plant Physiol.* **142**, 28-39.

Christodoulou, S., Joux, F., Marty, J.-C., Sempéré, R. and Rontani, J.-F. (2010) Comparative study of UV and visible light induced degradation of lipids in non-axenic senescent cells of *Emiliania huxleyi*. *Mar. Chem.* **119**, 139-152.

Collins, J.R., Edwards, B.R., Fredricks, H.F. and Van Mooy, B.A.S. (2016) LOBSTAHS: An adduct-based lipidomics strategy for discovery and identification of oxidative stress biomarkers. *Anal. Chem.* **88**, 7154-7162.

Collins, J.R., Edwards, B.R., Thamatrakoln, K., Ossolinski, J.E., DiTullio, G.R., Bidle, K.D., Doney, S.C. and Van Mooy, B.A.S. (2015) The multiple fates of sinking particles in the North Atlantic Ocean. *Global Biogeochem. Cycles* **29**, 1471-1494.

Cory, R.M., Ward, C.P., Crump, B.C. and Kling, G.W. (2014) Sunlight controls water column processing of carbon in arctic fresh waters. *Science* **345**, 925-928.

Cosgrove, J.P., Church, D.F. and Pryor, W.A. (1987) The kinetics of the autoxidation of polyunsaturated fatty acids. *Lipids* **22**, 299-304.

Crastes de Paulet, A., Douste-Blazy, L. and Paoletti, R. (1988) *Free Radicals, Lipoproteins, and Membrane Lipids*. Plenum Publishing Corporation, New York. 407 pp.

Cutignano, A., Lamari, N., d'Ippolito, G., Manzo, E., Cimino, G. and Fontana, A. (2011) Lipoxygenase products in marine diatoms: a concise analytical method to explore the functional potential of oxylipins. *J. Phycol.* **47**, 233-243.

Davidson, A.T., Bramich, D., Marchant, H.J. and McMinn, A. (1994) Effects of UV-B irradiation on growth and survival of Antarctic marine diatoms. *Mar. Biol.* **119**, 507-515.

Davidson, A.T. and Marchant, H.J. (1994) The impact of ultraviolet radiation on *Phaeocystis* and selected species of marine diatoms. In *Ultraviolet Radiation in Antarctica: Measurements and Biological Effects* (eds. C.S. Weiler and P.A. Penhale). American Geophysical Union, Washington, D.C.

Domingues, M.R.M., Reis, A. and Domingues, P. (2008) Mass spectrometry analysis of oxidized phospholipids. *Chem. Phys. Lipids* **156**, 1-12.

Domingues, M.R.M., Simões, C., da Costa, J.P., Reis, A. and Domingues, P. (2009) Identification of 1-palmitoyl-2-linoleoyl-phosphatidylethanolamine modifications under oxidative stress conditions by LC-MS/MS. *Biomed. Chromatogr.* **23**, 588-601.

Ducklow, H.W., Fraser, W.R., Meredith, M.P., Stammerjohn, S.E., Doney, S.C., Martinson, D.G., Sailley, S.F., Schofield, O.M., Steinberg, D.K., Venables, H.J. and Amsler, C.D. (2013) West Antarctic Peninsula: An ice-dependent coastal marine ecosystem in transition. *Oceanography* **26**, 190-203.

Ducklow, H.W., Schofield, O., Vernet, M., Stammerjohn, S. and Erickson, M. (2012) Multiscale control of bacterial production by phytoplankton dynamics and sea ice along the western Antarctic Peninsula: A regional and decadal investigation. *J. Mar. Syst.* **98–99**, 26-39.

Edwards, B.R., Bidle, K.D. and Van Mooy, B.A.S. (2015) Dose-dependent regulation of microbial activity on sinking particles by polyunsaturated aldehydes: Implications for the carbon cycle. *Proc Natl Acad Sci U S A* **112**, 5909-5914.

Edwards, B.R., Reddy, C.M., Camilli, R., Carmichael, C.A., Longnecker, K. and Van Mooy, B.A.S. (2011) Rapid microbial respiration of oil from the Deepwater Horizon spill in offshore surface waters of the Gulf of Mexico. *Environmental Research Letters* **6**.

Fahl, K. and Kattner, G. (1993) Lipid Content and fatty acid composition of algal communities in sea-ice and water from the Weddell Sea (Antarctica). *Polar Biol.* **13**, 405-409.

Falk-Petersen, S., Sargent, J.R., Henderson, J., Hegseth, E.N., Hop, H. and Okolodkov, Y.B. (1998) Lipids and fatty acids in ice algae and phytoplankton from the Marginal Ice Zone in the Barents Sea. *Polar Biol.* **20**, 41-47.

Feussner, I. and Wasternack, C. (2002) The lipoxygenase pathway. *Annu. Rev. Plant Biol.* **53**, 275-297.

Fichot, C.G. and Benner, R. (2014) The fate of terrigenous dissolved organic carbon in a river-influenced ocean margin. *Global Biogeochem. Cycles* **28**, 300-318.

Fontana, A., d'Ippolito, G., Cutignano, A., Miralto, A., Ianora, A., Romano, G. and Cimino, G. (2007) Chemistry of oxylipin pathways in marine diatoms. *Pure Appl. Chem.* **79**, 481-490.

Gardner, H.W. (1989) Oxygen radical chemistry of polyunsaturated fatty acids. *Free Radical Biology & Medicine* **7**, 65-86.

Girotti, A.W. (1990) Photodynamic lipid peroxidation in biological systems. *Photochem. Photobiol.* **51**, 497-509.

Girotti, A.W. (1998) Lipid hydroperoxide generation, turnover, and effector action in biological systems. *J. Lipid Res.* **39**, 1529-1542.

Girotti, A.W. (2001) Photosensitized oxidation of membrane lipids: reaction pathways, cytotoxic effects, and cytoprotective mechanisms. *J. Photochem. Photobiol. B: Biol.* **63**, 103-113.

Guschina, I.A. and Harwood, J.L. (2006) Lipids and lipid metabolism in eukaryotic algae. *Prog. Lipid Res.* **45**, 160-186.

Halliwell, B. and Chirico, S. (1993) Lipid peroxidation: Its mechanism, measurement, and significance. *Am. J. Clin. Nutr.* **57**, S715-S725.

Helbling, E.W., Eilertsen, H.C., Villafane, V.E. and Holm-Hansen, O. (1996) Effects of UV radiation on post-bloom phytoplankton populations in Kvalsund, north Norway. *Journal of Photochemistry and Photobiology B-Biology* **33**, 255-259.

Henderson, R.J. and Mackinlay, E.E. (1989) Effect of temperature on lipid composition of the marine cryptomonad *Chroomonas salina*. *Phytochemistry* **28**, 2943-2948.

Hessen, D.A.G., De Lange, H. and Van Donk, E. (1997) UV-induced changes in phytoplankton cells and its effects on grazers. *Freshwat. Biol.* **38**, 513-524.

Hoppe, H.-G. (1993) Use of fluorogenic model substrates for extracellular enzyme activity (EEA) measurement of bacteria. In *Handbook of Methods in Aquatic Microbial Ecology* (eds. P.F. Kemp, J.J. Cole, B.F. Sherr and E.B. Sherr). CRC Press, Boca Raton, Florida. pp. 423-431.

Hu, C., Muller-Karger, F.E. and Zepp, R.G. (2002) Absorbance, absorption coefficient, and apparent quantum yield: A comment on common ambiguity in the use of these optical concepts. *Limnol. Oceanogr.* **47**, 1261-1267.

Hummel, J., Segu, S., Li, Y., Irgang, S., Jueppner, J. and Giavalisco, P. (2011) Ultra performance liquid chromatography and high resolution mass spectrometry for the analysis of plant lipids. *Front Plant Sci* **2**.

Husen, P., Tarasov, K., Katafiasz, M., Sokol, E., Vogt, J., Baumgart, J., Nitsch, R., Ekroos, K. and Ejsing, C.S. (2013) Analysis of lipid experiments (ALEX): a software framework for analysis of high-resolution shotgun lipidomics data. *Plos One* **8**, e79736.

Intergovernmental Panel on Climate Change. (2005) Special report on safeguarding the ozone layer and the global climate system: Issues related to hydrofluorocarbons and perfluorocarbons.

Janero, D.R. (1990) Malondialdehyde and thiobarbituric acid-reactivity as diagnostic indices of lipid peroxidation and peroxidative tissue injury. *Free Radical Biol. Med.* **9**, 515-540.

Jankowski, J.J., Kieber, D.J. and Mopper, K. (1999) Nitrate and nitrite ultraviolet actinometers. *Photochem. Photobiol.* **70**, 319-328.

Karentz, D. (1994) Ultraviolet tolerance mechanisms in Antarctic marine organisms. In *Ultraviolet Radiation in Antarctica: Measurements and Biological Effects* (eds. C.S. Weiler and P.A. Penhale). American Geophysical Union, Washington, D.C.

Karl, D.M. and Resing, J. (1993) Palmer LTER: Hydrogen peroxide in the Palmer-LTER region: IV. Photochemical interactions with dissolved organic matter. *Antarct. J. U.S.* **28**.

Kawamura, K. and Gagosian, R.B. (1987) Implications of ω-oxocarboxylic acids in the remote marine atmosphere for photo-oxidation of unsaturated fatty acids. *Nature* **325**, 330-332.

Kawamura, K. and Gagosian, R.B. (1990) Mid-chain ketocarboxylic acids in the remote marine atmosphere: Distribution patterns and possible formation mechanisms. *Journal of Atmospheric Chemistry* **11**, 107-122.

Kessner, D., Chambers, M., Burke, R., Agus, D. and Mallick, P. (2008) ProteoWizard: open source software for rapid proteomics tools development. *Bioinformatics* **24**, 2534–2536.

Kieber, D.J., McDaniel, J. and Mopper, K. (1989) Photochemical source of biological substrates in sea water: implications for carbon cycling. *Nature* **341**, 637-639.

Kieber, D.J., Toole, D.A., Jankowski, J.J., Kiene, R.P., Westby, G.R., del Valle, D.A. and Slezak, D. (2007) Chemical "light meters" for photochemical and photobiological studies. *Aquat. Sci.* **69**, 360-376.

Kieber, R.J., Hydro, L.H. and Seaton, P.J. (1997) Photooxidation of triglycerides and fatty acids in seawater: Implication toward the formation of marine humic substances. *Limnol. Oceanogr.* **42**, 1454-1462.

Kim, H., Doney, S.C., Iannuzzi, R.A., Meredith, M.P., Martinson, D.G. and Ducklow, H.W. (2016) Climate forcing for dynamics of dissolved inorganic nutrients at Palmer Station, Antarctica: An interdecadal (1993–2013) analysis. *Journal of Geophysical Research: Biogeosciences* **121**, 2369-2389.

Kim, H. and Ducklow, H.W. (2016) A decadal (2002–2014) analysis for dynamics of heterotrophic bacteria in an Antarctic coastal ecosystem: Variability and physical and biogeochemical forcings. *Frontiers in Marine Science* **3**.

Kirk, J.T.O. (2011) *Light and Photosynthesis in Aquatic Ecosystems*, 3rd ed. Cambridge University Press, Cambridge.

Koppenol, W.H. (1990) Oxyradical reactions: from bond-dissociation energies to reduction potentials. *FEBS Lett.* **264**, 165-167.

Kramer, G.F., Norman, H.A., Krizek, D.T. and Mirecki, R.M. (1991) Influence of UV-B radiation on polyamines, lipid peroxidation and membrane lipids in cucumber. *Phytochemistry* **30**, 2101-2108.

Kuhl, C., Tautenhahn, R., Bottcher, C., Larson, T.R. and Neumann, S. (2012) CAMERA: an integrated strategy for compound spectra extraction and annotation of liquid chromatography/mass spectrometry data sets. *Anal. Chem.* **84**, 283-289.

Latch, D.E. and McNeill, K. (2006) Microheterogeneity of singlet oxygen distributions in irradiated humic acid solutions. *Science* **311**, 1743-1747.

Laube, J.C., Newland, M.J., Hogan, C., Brenninkmeijer, C.A.M., Fraser, P.J., Martinerie, P., Oram, D.E., Reeves, C.E., Rockmann, T., Schwander, J., Witrant, E. and Sturges, W.T. (2014) Newly detected ozone-depleting substances in the atmosphere. *Nature Geosci* **7**, 266–269.

Lauritano, C., Borra, M., Carotenuto, Y., Biffali, E., Miralto, A., Procaccini, G. and Ianora, A. (2011) Molecular evidence of the toxic effects of diatom diets on gene expression patterns in copepods. *Plos One* **6**, e26850.

Lauritano, C., Carotenuto, Y., Miralto, A., Procaccini, G. and Ianora, A. (2012) Copepod population-specific response to a toxic diatom diet. *Plos One* **7**, e47262.

Leflaive, J. and Ten-Hage, L. (2009) Chemical interactions in diatoms: role of polyunsaturated aldehydes and precursors. *New Phytol.* **184**, 794-805.

Lizotte, M.P. (2001) The contributions of sea ice algae to Antarctic marine primary production. *Am. Zool.* **41**, 57-73.

Marchand, D. and Rontani, J.-F. (2001) Characterisation of photo-oxidation and autoxidation products of phytoplanktonic monounsaturated fatty acids in marine particulate matter and recent sediments. *Org. Geochem.* **32**, 287-304.

Meredith, M.P. and King, J.C. (2005) Rapid climate change in the ocean west of the Antarctic Peninsula during the second half of the 20th century. *Geophys. Res. Lett.* **32**, L19604.

Milic, I., Fedorova, M., Teuber, K., Schiller, J. and Hoffmann, R. (2012) Characterization of oxidation products from 1-palmitoyl-2-linoleoyl-sn-glycerophosphatidylcholine in aqueous solutions and their reactions with cysteine, histidine and lysine residues. *Chem. Phys. Lipids* **165**, 186-196.

Miller, W.L. (1998) Effects of UV radiation on aquatic humus: Photochemical principles and experimental considerations. In *Aquatic Humic Substances: Ecology and Biogeochemistry* (eds. D.O. Hessen and L.J. Tranvik). Springer Berlin Heidelberg, Berlin. pp. 125-143.

Miralto, A., Barone, G., Romano, G., Poulet, S.A., Ianora, A., Russo, G.L., Buttino, I., Mazzarella, G., Laabir, M., Cabrini, M. and Giacobbe, M.G. (1999) The insidious effect of diatoms on copepod reproduction. *Nature* **402**, 173-176.

Mock, T. and Kroon, B.M.A. (2002) Photosynthetic energy conversion under extreme conditions—II: the significance of lipids under light limited growth in Antarctic sea ice diatoms. *Phytochemistry* **61**, 53-60.

Montes-Hugo, M., Doney, S.C., Ducklow, H.W., Fraser, W., Martinson, D., Stammerjohn, S.E. and Schofield, O. (2009) Recent changes in phytoplankton communities associated with rapid regional climate change along the Western Antarctic Peninsula. *Science* **323**, 1470-1473.

Moreau, S., Vidussi, F., Ferreyra, G. and Mostajir, B. (2016) Ecological impacts of ultraviolet-B radiation on marine ecosystems. In *Stressors in the Marine Environment* (eds. M. Solan and N. Whiteley). Oxford University Press, Oxford.

Murphy, T.M. (1983) Membranes as targets of ultraviolet radiation. *Physiol. Plant.* **58**, 381-388.

Neale, P.J., Lesser, M.P. and Cullen, J.J. (1994) Effects of ultraviolet radiation on the photosynthesis of phytoplankton in the vicinity of McMurdo Station, Antarctica. In *Ultraviolet Radiation in Antarctica: Measurements and Biological Effects* (eds. C.S. Weiler and P.A. Penhale). American Geophysical Union, Washington, D.C.

Nelson, J.R. (1993) Rates and possible mechanism of light-dependent degradation of pigments in detritus derived from phytoplankton. *Journal of Marine Research* **51**, 155-179.

Nichols, P.D., Palmisano, A.C., Rayner, M.S., Smith, G.A. and White, D.C. (1989) Changes in the lipid composition of Antarctic sea-ice diatom communities during a spring bloom: an indication of community physiological status. *Antarct. Sci.* **1**, 133-140.

O'Donnell, V.B. (2011) Mass spectrometry analysis of oxidized phosphatidylcholine and phosphatidylethanolamine. *Biochim. Biophys. Acta* **1811**, 818-826.

Palmisano, A.C., Lizotte, M.P., Smith, G.A., Nichols, P.D., White, D.C. and Sullivan, C.W. (1988) Changes in photosynthetic carbon assimilation in Antarctic sea-ice diatoms during spring bloom: variation in synthesis of lipid classes. *J. Exp. Mar. Biol. Ecol.* **116**, 1-13.

Patterson, L.K. and Hasegawa, K. (1978) Pulse radiolysis studies in model lipid systems: The influence of aggregation on kinetic behavior of OH-induced radicals in aqueous aodium linoleate. *Berichte der Bunsengesellschaft für physikalische Chemie* **82**, 951-956.

Perrette, M., Yool, A., Quartly, G.D. and Popova, E.E. (2011) Near-ubiquity of ice-edge blooms in the Arctic. *Biogeosciences* **8**, 515-524.

Popendorf, K.J., Fredricks, H.F. and Van Mooy, B.A.S. (2013) Molecular ion-independent quantification of polar glycerolipid classes in marine plankton using triple quadrupole MS. *Lipids* **48**, 185-195.

Prézelin, B.B., Boucher, N.P. and Smith, R.C. (1994) Marine primary production under the influence of the Antarctic ozone hole: Icecolors '90. In *Ultraviolet Radiation in Antarctica: Measurements and Biological Effects* (eds. C.S. Weiler and P.A. Penhale). American Geophysical Union, Washington, D.C. pp. 159-186.

Qian, J.G., Mopper, K. and Kieber, D.J. (2001) Photochemical production of the hydroxyl radical in Antarctic waters. *Deep-Sea Res Pt I* **48**, 741-759.

R Core Team (2016) R: a language and environment for statistical computing, version 3.4.0. R Foundation for Statistical Computing, Vienna, Austria.

Reis, A., Domingues, M.R.M., Amado, F.M.L., Ferrer-Correia, A.J.V. and Domingues, P. (2005) Separation of peroxidation products of diacyl-phosphatidylcholines by reversed-phase liquid chromatography–mass spectrometry. *Biomed. Chromatogr.* **19**, 129-137.

Reis, A. and Spickett, C.M. (2012) Chemistry of phospholipid oxidation. *Biochim. Biophys. Acta* **1818**, 2374-2387.

Ribalet, F., Intertaglia, L., Lebaron, P. and Casotti, R. (2008) Differential effect of three polyunsaturated aldehydes on marine bacterial isolates. *Aquat. Toxicol.* **86**, 249-255.

Rontani, J.-F. (1999) Photodegradation of lipidic compounds during the senescence of phytoplankton. In *Environmental Photochemistry* (ed. P. Boule). Springer Berlin Heidelberg, Berlin. pp. 263-284.

Rontani, J.-F. (2001) Visible light-dependent degradation of lipidic phytoplanktonic components during senescence: a review. *Phytochemistry* **58**, 187-202.

Rontani, J.-F., Belt, S.T., Brown, T.A., Amiraux, R., Gosselin, M., Vaultier, F. and Mundy, C.J. (2016) Monitoring abiotic degradation in sinking versus suspended Arctic sea ice algae during a spring ice melt using specific lipid oxidation tracers. *Org. Geochem.* **98**, 82-97.

Rontani, J.-F., Charriere, B., Forest, A., Heussner, S., Vaultier, F., Petit, M., Delsaut, N., Fortier, L. and Sempere, R. (2012a) Intense photooxidative degradation of planktonic and bacterial lipids in sinking particles collected with sediment traps across the Canadian Beaufort Shelf (Arctic Ocean). *Biogeosciences* **9**, 4787-4802.

Rontani, J.-F., Charriere, B., Petit, M., Vaultier, F., Heipieper, H.J., Link, H., Chaillou, G. and Sempere, R. (2012b) Degradation state of organic matter in surface sediments from the Southern Beaufort Sea: a lipid approach. *Biogeosciences* **9**, 3513-3530.

Rontani, J.-F., Cuny, P. and Grossi, V. (1998) Identification of a "pool" of lipid photoproducts in senescent phytoplanktonic cells. *Org. Geochem.* **29**, 1215-1225.

Roy, S. (2000) Strategies for the minimisation of UV-induced damage. In *The Effects of UV Radiation in the Marine Environment* (eds. S.J. de Mora, S. Demers and M. Vernet). Cambridge University Press, Cambridge. pp. 177-205.

Saba, G.K., Fraser, W.R., Saba, V.S., Iannuzzi, R.A., Coleman, K.E., Doney, S.C., Ducklow, H.W., Martinson, D.G., Miles, T.N., Patterson-Fraser, D.L., Stammerjohn, S.E., Steinberg, D.K. and Schofield, O.M. (2014) Winter and spring controls on the summer food web of the coastal West Antarctic Peninsula. *Nature Communications* **5**, 4318.

Sala, P., Pötz, S., Brunner, M., Trötzmüller, M., Fauland, A., Triebl, A., Hartler, J., Lankmayr, E. and Köfeler, H. (2015) Determination of oxidized phosphatidylcholines by hydrophilic interaction liquid chromatography coupled to Fourier Transform mass spectrometry. *International Journal of Molecular Sciences* **16**, 8351.

Santos, A.L., Henriques, I., Gomes, N.C.M., Almeida, A., Correia, A. and Cunha, A. (2011) Effects of ultraviolet radiation on the abundance, diversity and activity of bacterioneuston and bacterioplankton: insights from microcosm studies. *Aquat. Sci.* **73**, 63-77.

Schaich, K.M. (2005) Lipid oxidation: Theoretical aspects. In *Bailey's Industrial Oil and Fat Products*. John Wiley & Sons, Inc.

Schofield, O., Kroon, B.M.A. and Prézelin, B.B. (1995) Impact of ultraviolet-B radiation on photosystem II activity and its relationship to the inhibition of carbon fixation rates for Antarctic ice algae communities. *J. Phycol.* **31**, 703-715.

Schofield, O., Saba, G., Coleman, K., Carvalho, F., Couto, N., Ducklow, H., Finkel, Z., Irwin, A., Kahl, A., Miles, T., Montes-Hugo, M., Stammerjohn, S. and Waite, N. (2017) Decadal variability in coastal phytoplankton community composition in a changing West Antarctic Peninsula. *Deep Sea Research Part I: Oceanographic Research Papers* **124**, 42-54.

Skerratt, J.H., Davidson, A.D., Nichols, P.D. and McMeekin, T.A. (1998) Effect of UV-B on lipid content of three Antarctic marine phytoplankton. *Phytochemistry* **49**, 999-1007.

Smith, C.A., Want, E.J., O'Maille, G., Abagyan, R. and Siuzdak, G. (2006) XCMS: processing mass spectrometry data for metabolite profiling using nonlinear peak alignment, matching, and identification. *Anal. Chem.* **78**, 779–787.

Smith, D.C. and Azam, F. (1992) A simple, economical method for measuring bacterial protein synthesis rates in seawater using ^{3}H-leucine. *Mar. Microb. Food Webs* **6**, 107-114.

Smith, W.O. (1987) Phytoplankton dynamics in marginal ice zones. *Oceanogr. Mar. Biol. Annu. Rev.* **25**, 11-38.

Smith, W.O. and Nelson, D.M. (1985) Phytoplankton bloom produced by a receding ice edge in the Ross Sea: Spatial coherence with the density field. *Science* **227**, 163-166.

Smith, W.O. and Nelson, D.M. (1986) Importance of ice edge phytoplankton production in the Southern Ocean. *Bioscience* **36**, 251-257.

Solomon, S., Ivy, D.J., Kinnison, D., Mills, M.J., Neely, R.R. and Schmidt, A. (2016) Emergence of healing in the Antarctic ozone layer. *Science* **353**, 269-274.

Spickett, C.M. and Pitt, A.R. (2015) Oxidative lipidomics coming of age: advances in analysis of oxidized phospholipids in physiology and pathology. *Antioxid Redox Sign* **22**, 1646-1666.

Spickett, C.M., Reis, A. and Pitt, A.R. (2011) Identification of oxidized phospholipids by electrospray ionization mass spectrometry and LC-MS using a QQLIT instrument. *Free Radical Biol. Med.* **51**, 2133-2149.

Sumner, L., Amberg, A., Barrett, D., Beale, M., Beger, R. and Daykin, C. (2007) Proposed minimum reporting standards for chemical analysis. *Metabolomics* **3**, 211–221.

Tautenhahn, R., Boettcher, C. and Neumann, S. (2008) Highly sensitive feature detection for high resolution LC/MS. *BMC Bioinformatics* **9**, 504.

Vähätalo, A.V., Salkinoja-Salonen, M., Taalas, P. and Salonen, K. (2000) Spectrum of the quantum yield for photochemical mineralization of dissolved organic carbon in a humic lake. *Limnol. Oceanogr.* **45**, 664-676.

Vernet, M., Brody, E.A., Holm-Hansen, O. and Mitchell, B.G. (1994) The response of Antarctic phytoplankton to ultraviolet radiation: Absorbtion, photosynthesis, and taxonomic composition. In *Ultraviolet Radiation in Antarctica: Measurements and Biological Effects* (eds. C.S. Weiler and P.A. Penhale). American Geophysical Union, Washington, D.C.

Vernet, M., Martinson, D., Iannuzzi, R., Stammerjohn, S., Kozlowski, W., Sines, K., Smith, R. and Garibotti, I. (2008) Primary production within the sea-ice zone west of the Antarctic Peninsula: I-Sea ice, summer mixed layer, and irradiance. *Deep-Sea Res Pt II* **55**, 2068-2085.

Vu, H.S., Tamura, P., Galeva, N.A., Chaturvedi, R., Roth, M.R., Williams, T.D., Wang, X., Shah, J. and Welti, R. (2012) Direct infusion mass spectrometry of oxylipin-containing *Arabidopsis* membrane lipids reveals varied patterns in different stress responses. *Plant Physiol.* **158**, 324-339.

Wagner, B.A., Buettner, G.R. and Burns, C.P. (1994) Free radical-mediated lipid peroxidation in cells: Oxidizability is a function of cell lipid *bis*-allylic hydrogen content. *Biochemistry* **33**, 4449-4453.

Ward, C.P., Nalven, S.G., Crump, B.C., Kling, G.W. and Cory, R.M. (2017) Photochemical alteration of dissolved organic carbon draining permafrost soils shifts microbial metabolic pathways and stimulates respiration. *Nature Communications* **8**, 772. https://doi.org/10.1038/s41467-017-00759-2

Warnes, G.R., Bolker, B., Bonebakker, L., Gentleman, R., Huber, W., Liaw, A., Lumley, T., Maechler, M., Magnusson, A., Moeller, S., Schwartz, M. and Venables, B. (2016) gplots: Various R Programming Tools for Plotting Data. R package, version 3.0.1.

Wichard, T., Poulet, S.A. and Pohnert, G. (2005) Determination and quantification of alpha-, beta-, gamma-, and delta-unsaturated aldehydes as pentafluorobenzyl-oxime derivates in diatom cultures and natural phytoplankton populations: application in marine field studies. *Journal of Chromatography B-Analytical Technologies in the Biomedical and Life Sciences* **814**, 155-161.

Worrest, R.C. (1983) Impact of solar ultraviolet-B radiation (290-320 nm) upon marine microalgae. *Physiol. Plant.* **58**, 428-434.